4

Surface Plasmon Resonance Biosensing in the Study of Ternary Systems of Interacting Proteins

Eric J. Sundberg, Peter S. Andersen, Inna I. Gorshkova, and Peter Schuck*

4.1. INTRODUCTION

Surface plasmon resonance (SPR) biosensors are optical evanescent wave sensors, where light in total internal reflection is used to probe properties of the solution adjacent to the surface. SPR occurs through the interaction of light with a thin metal film, which can be used to measure the refractive index of the solution close to the surface with high sensitivity (Kretschmann and Raether, 1968; Knoll, 1998). This is exploited in the study of protein interactions by immobilizing one binding partner to the surface, and observing the change in local refractive index during the interaction with a label-free soluble-binding partner.

SPR technology became a popular tool for studying protein interactions in the 1990s with the introduction of commercial instruments. It is closely related in many ways to the optical biosensor techniques described in Chapter 3. Nevertheless, the widespread availability, the versatility of this approach, and the many published applications of qualitative and quantitative binding studies warrant a separate chapter on the potential of SPR biosensors in the study of complex systems of interacting proteins. This chapter is not intended to be an exhaustive review, but is

E. J. SUNDBERG • Boston Biomedical Research Institute, Watertown, MA, USA. P. S. ANDERSEN • Symphogen A/S, Copenhagen, Denmark. I. I. GORSHKOVA • National Institute for Biomedical Imaging and Bioengineering, National Institutes of Health, Bethesda, MD, USA. P. SCHUCK • National Institute for Biomedical Imaging and Bioengineering, National Institutes of Health, 13 South Drive, Bethesda, MD 20892 and *Corresponding author: Tel: +1 301 4351950; fax: +1 301 4801242; e-mail: pschuck@helix.nih.gov

instead meant to critically highlight only certain features and selected approaches for the analysis of multiprotein complexes. For more general information, practical protocols, or literature reviews highlighting other topics, the reader is referred to many published reviews (e.g., O'Shannessy, 1994; Malmborg and Borrebaeck, 1995; van der Merwe and Barclay, 1996; Schuck, 1997b; Huber *et al*., 1999; Hall, 2001; Cooper, 2002; Alves *et al*., 2005; Lee *et al*., 2005; Pattnaik, 2005).

It has been generally recognized that, when SPR biosensors were first commercially introduced, the interpretation of the surface-binding kinetic traces was frequently too simplistic, and based in many cases on unwarranted assumptions regarding the ideality of the measurement and the information content of the recorded traces (Schuck, 1997a). However, as many elegant and well-controlled SRP studies in the literature have demonstrated, this should not detract from the possibility to use SPR technology as a reliable biophysical research tool, since knowledge about experimental and analytical aspects available have evolved significantly since the initial introduction. SPR is extremely flexible in the experimental setup, and very useful for studying many facets of multiprotein complex formation. In particular, in the context of a combination with other biophysical tools, it can provide unique and reliable information.

From the perspective of studying reversibly associating proteins, there are several essential aspects of SPR biosensing that should be noted in comparison with solution-based methods. First, for characterizing reversible interactions, the surface immobilization eliminates the need to work with both proteins at concentrations close to the order of magnitude of the binding constant (K_D). Instead, the surface concentration of the immobilized protein can be chosen to optimize the magnitude of the signal, whereas the soluble-binding partner is typically in the range of 0.1–10-fold the K_D. Only the concentration of the soluble species governs the fractional saturation of sites. This permits the study of reversible, very high affinity interactions without running into problems of either too low signal or entirely stoichiometric binding. In principle, interactions with affinities spanning a range of at least 10^4–$10^{10}\,M^{-1}$ can be characterized by SPR. Of course, surface immobilization may introduce problems itself because of chemical modification and conformational constraints. Several commonly used approaches will be described later. In addition, the properties of the surface itself need to be considered when interpreting the binding experiments. Different strategies addressing this problem, such as the use of reference surfaces and competition-binding approaches, will be discussed.

A second essential feature of SPR biosensing is the ability to observe in real time the kinetics of the surface-binding process. When the soluble-binding partner is injected into the flow across the sensor surface, its time course of accumulation at the surface sites and the attainment of a steady state can usually be readily observed, as well as the dissociation of the complex after chasing the surface with a flow of buffer. This has great potential for the elucidation of the binding kinetics of interacting proteins, for which chemical association rates of up to 10^5–$10^6\,M^{-1}s^{-1}$ and dissociation rates of between 10^{-5} and $10^{-1}\,s^{-1}$ are generally accessible.

In principle, this can also permit the estimation of equilibrium constants even in the absence of reaching true steady state, even though there are special considerations and precautions needed for this extrapolation because of the macroscopic transport of soluble analyte from the flow to the sensor surface. This can be particularly advantageous in situations in which protein quantities are limited, or where the equilibration time is impractically long.

Third, the biosensor surface can act effectively as a miniaturized affinity chromatography matrix, allowing for the separation of unbound soluble protein, or any other contaminating or nonparticipating molecules, from the surface-bound complex. For systems with slow dissociation rates, this has preparative implications, as the amount of material captured can be compatible with mass spectroscopy. It also has important analytical consequences, since the preformed surface-bound complex is available for further investigation by probing binding with a third protein species, which can be a powerful tool for qualitative or quantitative studies of multiprotein complexes.

In this chapter, we will (1) describe the basic principles of SPR detection, a variety of strategies for functional attachment of proteins to the sensor surface, and summarize some standard kinetic and thermodynamic experiments for binary protein interactions; (2) outline a set of experimental restrictions and controls that are aimed at ensuring the absence of characteristic artifacts arising from using surface binding as a probe for protein interactions; (3) illustrate the capacity of SPR biosensing in multiprotein interactions or interactions with multiple conformations and cooperativity; and (4) provide a selective literature review of practical applications to different types of interacting protein systems, focusing largely on the ternary complex formation between bacterial superantigen (SAG), T-cell receptor (TCR), and major histocompatibility complex (MHC) molecules (Andersen *et al.*, 2002).

4.2. SURFACE PLASMON RESONANCE BASICS

4.2.1. Physical Principle

The SPR biosensor experiment exploits surface-confined electromagnetic fields for real-time measurement of the refractive index of the medium in the immediate vicinity of the sensor surface (Kretschmann and Raether, 1968; Raether, 1977; Lukosz, 1991; Garland, 1996; Knoll, 1998). An evanescent wave is created when light strikes the interface between the glass of a sensor surface and the assay buffer at an angle in total internal reflection. The typical decay length of the evanescent field for visible light is on the order of a few hundred nanometers. If a thin metal layer is located at the interface, the light can cause surface charge density waves (surface plasmons) in the free electrons on the metal film. For a specific angle of incidence of the light, the wave vector of the reflected light and the surface plasmons are in phase, and resonant energy transfer can take place,

which diminishes the intensity of the reflected light. This is called SPR. Since the angle of minimum reflectivity depends strongly on the refractive index of the solution in the vicinity of the sensor surface, the analysis of the angular-dependent reflectivity can be used to determine this refractive index with a precision of up to 6–7 decimal places. Thus, even though the refractive index increment of proteins is only 0.15–0.19 ml/g, and thus not dramatically different from water and not a highly sensitive parameter, protein accumulation on the sensor surface can be followed with high precision via the concurrent local increase of refractive index.

Other optical evanescent wave sensors are based on waveguide principles, where a thin high-refractive index layer is deposited on the interface. This permits the detection of phase shifts of the guided light in two polarizations, both having different decay lengths of the evanescent field, which in combination gives information about the effective average layer thickness of a protein film in addition to the refractive index (Lukosz, 1991). Even though these approaches yield a richer data basis on protein interactions, and can provide information on conformational changes (Salamon *et al*., 1994, 1998), they so far did not have as widespread applications as SPR (for a more detailed review, see Alves *et al*., 2005). Several other label-free optical techniques for assessing surface-bound protein have been developed (see Brecht and Gauglitz (1995), Chapter 3, and references cited therein). This also includes high-throughput formats and imaging techniques. The following discussion is restricted to SPR, but many aspects apply directly to other evanescent wave biosensors, as well.

Figure 4.1A shows the basic idea of a surface-binding experiment. In the SPR instrument from Biacore AB (www.biacore.com), sample is supplied in microfluidic channels containing an HPLC-like injection loop (Sjölander and Urbaniczky, 1991). Alternative approaches eliminating the constraints from the finite volume of the sample plug (and the resulting limitation in contact time and flow rate of the sample with the sensor surface) have been reported using cuvette-type systems (such as the IAsys instrument from Thermo, UK), circulating sample (Schuck *et al*., 1998), and oscillating flow (Abrantes *et al*., 2001), the latter combining a significant reduction of sample volume with high flow rates and extended observation time (Abrantes *et al*., 2001). In any case, the change in reflectivity, caused by the binding or dissociation of molecules from the sensor surface, is in first approximation proportional to the mass of bound material and is recorded in a so-called sensorgram (Figure 4.1B). After (usually covalent) immobilization of one binding partner to the surface, the sensorgram permits following in real time the increasing response as molecules dissolved in the sample flowing across the surface interact with the surface sites. The response remains constant if the interaction attains a steady state. When sample flow is replaced by buffer, the response decreases as the interacting-binding partners dissociate and the soluble molecule is released from the surface. The signal from bulk refractive changes is measured separately on a similarly treated but nonfunctionalized surface, and subtracted from the traces to be analyzed (Ober and Ward, 1999a; Karp *et al*., 2005). The analysis of the net binding traces can be used to derive information on kinetic rate constants and equilibrium

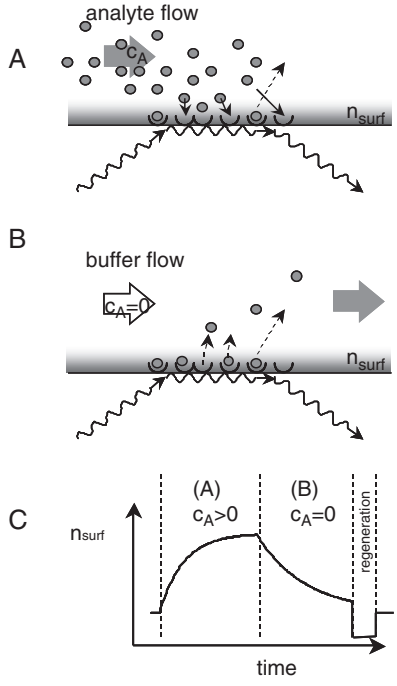

Figure 4.1. Schematic presentation of a typical optical biosensor experiment. Light is coupled into a structure that allows generation of surface-confined electromagnetic waves, which are sensitive to the refractive index of the solution close to the surface, n_{surf}, in the range of the evanescent field. Typical penetration depths of the sensitive volume into the solution are in the order of 100 nm. Ligands are attached to the sensor surface, as indicated by half-circles. (A) When analytes (full circles) are introduced into the solution above the surface, reversible interactions with the ligand leads to binding and dissociation events. (B) When the surface is washed by running buffer in the absence of analyte, only dissociation events take place. (C) Signal obtained from probing the refractive index n_{surf} during the sequential application of the configurations depicted in A and B, given in arbitrary units. Following the association phase (A) and the dissociation phase (B), usually a regeneration procedure is applied for removing the remaining analyte from the surface before a new experimental cycle takes place.

constants of the interaction. The following section will outline some of the fundamental aspects of such experiments.

4.2.2. Immobilization

The goal of immobilization is the stable coupling of the ligand to the sensor surface in its active form. To prevent irreversible adsorption of protein to the metal film, the surface can be coated with self-assembled monolayer of alkyl-thiols (Löfås and Johnsson, 1990). Further, in many cases, a sensor surface is chosen that is coated with a polymer, such as carboxymethyl dextran, in order to serve as an immobilization matrix and to suppress nonspecific interactions (Löfås and

Johnsson, 1990). Several methods exist for immobilization of ligand to the sensor chip surface (O'Shannessy *et al*., 1992). The strategy of immobilization is related to the choice of the regeneration procedure for the surface, which is frequently required to strip remaining bound protein from the surface before starting a new cycle of association and dissociation. For an overview and practical protocols, see Schuck *et al*. (1999).

The most commonly used procedure is to covalently couple molecules to a carboxymethyl dextran-coated sensor surface via amine, thiol, aldehyde, or carboxyl groups. It should be noted that these immobilization methods differ in their exposure of the ligand to relatively harsh conditions. Electrostatic preconcentration of protein below its p*I* under low salt conditions in the negatively charged carboxymethyl dextran can provide highly effective immobilization requiring only microgram amounts of protein (Johnsson *et al*., 1991).

Other approaches rely on capturing the ligand noncovalently with another (covalently immobilized) protein, such as an antibody, protein A, or streptavidin, or capture of polyhistidine tags (Lata and Piehler, 2005). An elegant capture method for glycosylated proteins can be the use of lectins, such as concanavalin A, which recognize polysaccharides. This has been applied, for example, to the surface attachment of detergent-solubilized rhodopsin (Rebois *et al*., 2002; Northup, 2004).

For membrane receptors, techniques have been developed for creating supported or tethered planar lipid bilayers on the sensor surface (Atanasov *et al*., 2005; Tanaka and Sackmann, 2005). Proteins may be inserted into the bilayers or cross-linked to the lipid head groups (Cornell *et al*., 2001). This can provide lateral mobility and establish rotational preorientation of the molecules, which may profoundly influence the binding kinetics and thermodynamics. An example for a study of ligand interactions with extracellular receptor domains attached to supported lipid bilayers can be found in Chapter 3 on optical biosensors. Alternatively, hybrid bilayers consisting of surface-attached alkanethiol monolayers and phospholipid have been developed (Plant *et al*., 1995). Establishing methods for functional reconstitution of integral membrane proteins in supported lipid bilayers is a subject of intense current research. Techniques for the deposition of whole membrane fragments have been described (Rao *et al*., 1997).

Some of the chemical methods will result in cross-links to the surface in many different orientations. The site-specific capture or cross-link is usually preferable, even though it may be unclear if the physical orientation at the surface is uniform, for example, due to random immobilization applied to the capturing molecule.

Clearly, the choice of immobilization methods is specific to the molecular system studied. Regardless of which method is chosen, it is of paramount importance to control the number of available surface-binding sites, or the average immobilized ligand density, as numerous surface-related artifacts may be invoked if the surface density is too high (one is described Section 4.2). This density of immobilized ligand can be measured as the difference in the SPR signal before and after the immobilization procedure, which also provides an estimation of the maximal analyte-binding capacity. For kinetic experiments, the immobilized ligand

density should be maintained at a relatively low level, with the maximal binding capacity on the order of 50–200-fold the instrument noise. Another reason for maintaining low surface density of immobilized proteins may be the concern for some systems that the relatively high local concentration in the immobilization matrix may promote oligomerization or aggregation. In this case, comparison with binding studies in the opposite orientation, or with solution competition assays (see later), may be useful diagnostic tools.

As is apparent from the similarity of a flow-based biosensor surface with an affinity chromatographic matrix (Winzor, 2000), the largest difference being in the scale and the ability of real-time detection of bound analyte, the biosensor surface can serve an additional preparative function. The amounts of surface-bound material can be compatible with mass spectroscopic detection. Practical approaches have been developed to achieve recovery of the captured analyte and delivery to a mass spectrometer from SPR and other detectors, with different efficiency and sensitivity (Krone *et al*., 1997; Sonksen *et al*., 1998; Natsume *et al*., 2000, 2002; Gilligan *et al*., 2002; Mehlmann *et al*., 2005). The use of biosensors in affinity purification step can be superior to immunoprecipitation and conventional affinity chromatography with regard to the quality of the capture process (Williams and Addona, 2000). This can permit the identification of the soluble-binding partners from a mixture exposed to the sensor surface, and determine possible protein modifications essential for binding.

4.2.3. Binding Analysis

Although the interpretation may require consideration of different processes, the typical SPR experiments produce data that are highly quantitative and reproducible. The following describes a bimolecular reaction of a soluble analyte with the surface-immobilized ligand. If the analyte concentration c is held constant, for example, due to a replenishing with a flow or due to a negligible number of surface-bound analyte molecules, the binding progress $s(t)$ follows the rate equation

$$\frac{\mathrm{d}s}{\mathrm{d}t} = k_{\mathrm{on}} c(s_{\max} - s) - k_{\mathrm{off}} s, \tag{4.1}$$

where $s_{\max}$ denotes the signal at full saturation, and k_{on} and k_{off} the chemical on- and off-rate constants, with $K_{\mathrm{A}} = k_{\mathrm{on}}/k_{\mathrm{off}}$. If we apply the analyte at time t_0 for a contact time t_{c}, we can integrate the rate equation and arrive at the binding progress in the association phase

$$s_{\mathrm{a}}(c,t) = s_{\mathrm{eq}}(c)\left(1 - \mathrm{e}^{-(k_{\mathrm{on}}c + k_{\mathrm{off}})(t-t_0)}\right) \tag{4.2}$$

with the steady-state response

$$s_{\mathrm{eq}}(c) = \frac{s_{\max}}{1 + (K_{\mathrm{A}}c)^{-1}} \tag{4.3}$$

(Langmuir, 1918). After the analyte is removed, we see dissociation of the bound analyte from the surface with

$$s_d(c,t) = s_a(c,t_c)e^{-k_{off}(t-t_0+t_c)}. \quad (4.4)$$

Both association and dissociation are proportional to s_{max}, and are single exponential, ascending or descending traces. Thus, information content on the kinetic rate constants is present mostly in the curvature of the sensorgrams (corresponding, e.g., to the analysis of molar masses in sedimentation equilibrium, Chapter 10), and sufficiently long observation times are required. With the commercial SPR systems, baseline stability is usually sufficiently high for experiments over several hours or more. Typically, a nonlinear regression to globally fit the kinetic-binding curves obtained at different loading concentrations results in the most robust estimates of rate constants (O'Shannessy *et al*., 1993; Morton *et al*., 1995). Ober and Ward (1999b) have determined the limitations of accuracy of the kinetic constants that can be obtained from noisy SPR data. They have also demonstrated the application of a subspace algorithm, a new noniterative technique to directly fit exponential data, to SPR analysis (Ober *et al*., 2003).

Unfortunately, for reasons outlined later, the observation of binding kinetic data—with injection times and binding capacity appropriate for detailed kinetic modeling—that strictly follows Eqs. (4.3) and (4.4) is very rare (Karlsson *et al*., 1994; Schuck *et al*., 1998), despite the common uncritical use of this model in the past literature (Figure 4.2A). Nevertheless, the single-exponential binding is very important as a theoretically ''ideal'' case, against which experimental curves can be compared.

Alternatively, the equilibrium-binding constant can be derived from the concentration dependence of the steady-state signal, $s_{eq}(c)$, which follows a Langmuir isotherm (Eq. (4.3) and Figure 4.2B). This approach has the fundamental advantage that it is completely independent of the kinetic pathway, simplifying the analysis considerably. This consideration can be important in the study of more complex interactions (see later). In addition, the surface can be titrated in a configuration not requiring surface regeneration (Schuck *et al*., 1998; Abrantes *et al*., 2001).

A third very basic and highly useful type of experiment is the competition of surface binding with soluble forms of the surface-immobilized molecule. This approach uses the fact that the solution interaction leaves only a fraction of molecules free to interact with the surface sites. In the flow system, the contact time of the soluble mixture with the surface is typically too short, and the number of surface-binding molecules is typically too low, to warrant corrections in the equilibrium of the soluble molecules due to depletion caused by surface binding, even though numerical corrections can be applied. For a 1:1 interaction, the concentration of unbound protein can be calculated as

$$[A]_{free} = [A]_0 - 0.5\left\{[B] + [A]_0 + \frac{1}{K_{AB}} - \left(\left([B] + [A]_0 + \frac{1}{K_{AB}}\right)^2 - 4[B][A]_0\right)^{0.5}\right\} \quad (4.5)$$

with $[A]_{free}$ and $[A]_0$ denoting the free and the total of a soluble protein ''A'', interacting in equilibrium with a soluble protein ''B'' at concentration [B], and the

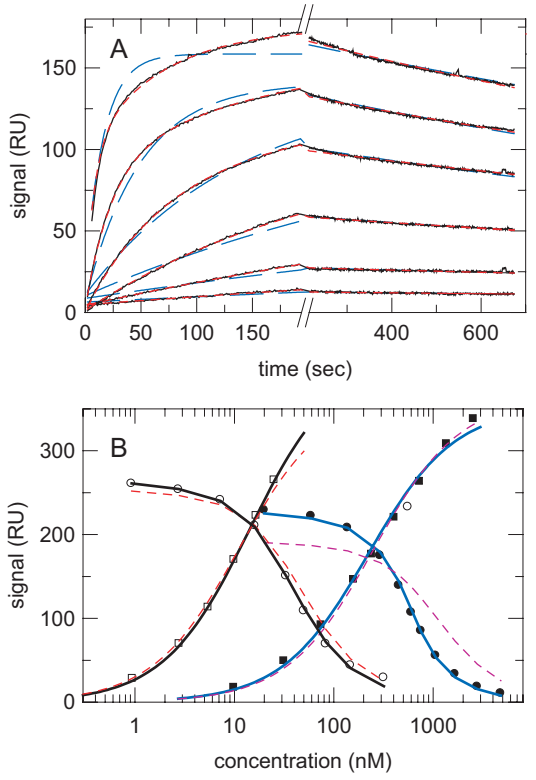

Figure 4.2. (A) Kinetic surface-binding traces of myoglobin binding to a surface-immobilized antibody, at concentrations between 4.6 and 990 nM (black lines), and global fit using a two-site model (red dotted line). For this interaction, in contrast to the data shown in this figure, Roden and Myszka (1996) presented a data set comprising of shorter contact times (<50 s) and a limited concentration range (maximum concentration 330 nM) and concluded that the interaction follows an ideal 1:1 reaction (Roden and Myszka, 1996). While such truncated data could be well-reproduced with the present surface, the best-fit single-site model to the present, more comprehensive, data set, however, is shown as blue dashed lines, clearly incompatible with the data. This highlights the necessity of collecting data with high information content (from sufficient signal/noise ratio and traces with significant curvature) to permit discrimination between different models for the surface-binding process and to arrive at a qualitatively and quantitatively reliable interpretation. For details, see Schuck *et al*. (1998). (B) Equilibrium surface-binding signals (squares) from equilibrium titration (Schuck *et al*., 1998) for the interaction of NC10 Fab to immobilized whale neuraminidase (filled symbols) and immobilized tern neuraminidase (open symbols). The solution competition isotherm using a fixed concentration of NC10 and variable soluble neuraminidase competing with the surface sites is shown as circles. The best-fit analysis allowing for different binding constants in solution and at the surface is shown as solid lines, and the global fit assuming the affinity to be identical in the solution and at the surface is shown as dotted lines. For whale neuraminidase, this suggests the solution interaction to be ~five-fold stronger, while for immobilized tern neuraminidase the surface- and the solution-binding constants are virtually identical. For details, see Schuck *et al*. (1998).

isotherm from the concentration dependence of the free soluble analyte binding to the surface sites can be quantitatively analyzed (Figure 4.2B). Further, the surface-binding properties of the soluble analyte can be empirically characterized (e.g., using a calibration curve for either the steady-state binding or the initial slopes), and the interaction with the immobilized surface site can be understood solely as a means to generate a concentration-dependent signal. In this way, this approach allows the probing of protein interactions in a manner entirely free from potential artifacts due to surface immobilization. A combination of both approaches permits probing whether the affinity of the surface sites is affected because of conformational constraints or the microenvironment at the surface (Figure 4.2B).

4.3. LIMITATIONS OF USING SURFACE-IMMOBILIZED SITES TO STUDY PROTEIN–PROTEIN INTERACTIONS

Besides the advantageous features of using biosensors for studying protein interactions outlined earlier, they also impose certain restrictions and difficulties that arise fundamentally from the fact that the sites are localized to the surface, beyond the potential problem of functional protein immobilization. These include mass transport limitations and the analysis of multivalent analytes. Although both the role of ligand diffusion to a cell-surface receptor, lateral receptor interactions in the plane of the membrane, as well as multivalent binding may be very important factors, or perhaps sometimes even govern, the process to effect a biological function *in vivo*, the correspondence of a cell surface *in vivo*, and the SPR biosensor surface is very difficult to establish. For example, the precise replication of the surface density, the lateral distribution and mobility in the plane of the surface is not possible, although they greatly influence the effects of multivalent attachment and mass transport. Likewise, the detailed physicochemical properties of the surface and the adjacent environment can be expected to exert a great influence on mass transport. Therefore, unless a well-controlled biophysical model system can be established, for example, such as described in Chapter 3, it seems usually advantageous to attempt to use the SPR sensor as a tool to characterize the interactions in solution, and to conduct the experiment under conditions free of surface-related effects, governed only by the association and dissociation events arising from the forces between protein interfaces and not from their spatial location. Understanding the dynamics of these processes will shed light on the properties of the proteins, and serve as a basis for studying their function in the biological context. This is obviously the goal also for the study of protein interactions that take place between soluble molecules away from any surface.

4.3.1. Multivalent Analytes

A classic example of a multivalent analyte is a full-length I_gG antibody. If we consider a bivalent antibody interacting with antigen immobilized to the sensor

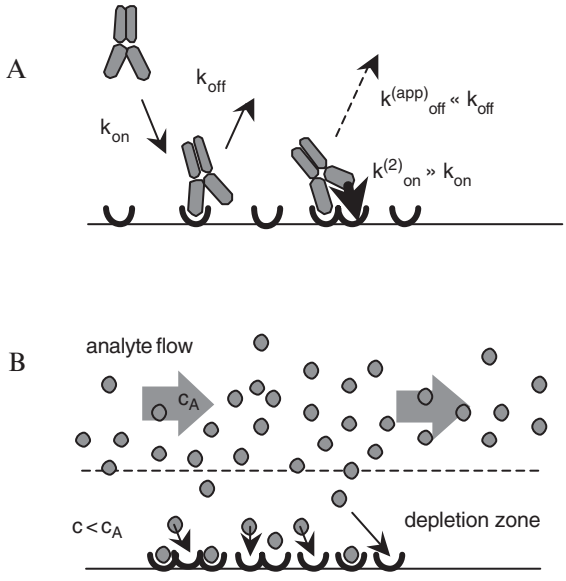

Figure 4.3. Experimental configurations of binding studies with surface-immobilized proteins exhibiting fundamental difficulties include (A) multivalent soluble analytes and (B) binding with rapid chemical kinetics and slow transport rate constants.

surface (Figure 4.3A), it may be bound either through one or through both combining sites, and since the SPR signal is sensitive essentially only to the total protein mass residing within the evanescent field, both states are indistinguishable. For an antibody molecule that has formed only a single antibody–antigen interface, but where a free antigen molecule is within accessible radius of the second combining site, the probability of making the second interaction is greatly enhanced over the probability of making the first interaction. At the same time, for the doubly bound molecule to be released from the surface requires simultaneous dissociation of both bonds, which is a statistically rare event compared with the dissociation of only one bond. Both effects strongly stabilize the surface-bound molecule, and, as a consequence, the apparent off-rate constant of whole antibody molecules dissociating from the antigen surface is frequently many orders of magnitudes slower than that of the individual antibody–antigen interfaces. The apparent K_D values may be many orders of magnitude lower than the true K_D (Ladbury *et al*., 1995).

The computational modeling of this effect has proven very difficult due to the dependence on the spatial distribution of the surface-immobilized antigen, and this is compounded by the fact that the use of a flexible matrix for surface immobilization introduces many additional variables (Nieba *et al*., 1996; Muller *et al*., 1998). A possible experimental approach is the use of very low density surface immobilization, to minimize the probability of simultaneous binding of both antibody-combining sites, but it seems problematic to establish to what degree this

approach is successful, since it would require spatially uniform immobilization (Nieba *et al*., 1996). While the total amount of surface-immobilized antigen that can be controlled, it is notoriously difficult to control or even measure the spatial distribution, in particular when using an extended polymer, such as the popular carboxymethyl dextran, as an immobilization matrix.

As a consequence, the best method to reliably avoid this artifact and to permit a quantitative thermodynamic or kinetic analysis of the interaction is to immobilize the multivalent species and use soluble analytes that are only monovalent with regard to the surface-immobilized species. This also rules out the use of self-associating species as a soluble analyte, and makes very difficult the quantitative study of homogeneous protein self-association processes. However, it may be used, for example, in some configurations to characterize the process of subunit dissociation after selective immobilization of oligomeric complexes, or in fibrillation processes for the association and the dissociation of monomers to and from surface-immobilized nuclei or fibers (Hasegawa *et al*., 2002).

The same restriction also imposes stringent requirements for sample preparation. Even at low levels, soluble oligomeric aggregates can accumulate at the sensor surface, and have been found to have considerable influence on the apparent association and dissociation kinetics. If unrecognized oligomeric impurities are present, this may lead to biphasic binding and dissociation curves, and cause significant deviations of binding constants. Depending on the size of the analyte, size-exclusion chromatography may be used to ensure the absence of relatively stable oligomeric aggregates (Davis *et al*., 1998; Andersen *et al*., 1999; Schuck *et al*., 1999). As an analytical tool, sedimentation velocity analytical ultracentrifugation (see Chapter 16) is playing an important role in the highly sensitive detection of oligomers and larger aggregates below the 1% level. These may be a result of imperfect refolding of proteins, protein degradation, or low-level aggregation after protein freeze–thaw cycles. Sedimentation velocity is also a reliable tool for the detection and the characterization of reversible oligomerization.

4.3.2. Mass Transport Limitation

Transport limitation arises as a consequence of the experimental configuration in which the soluble analyte is initially not mixed well with the immobilized sites at the start of the binding experiments, and of the requirement to hold the analyte concentration constant during the experiment. If the macroscopic supply of analyte to the sensor surface is not sufficiently fast compared with the chemical reaction, the observed surface-binding kinetics reflects the characteristics of this transport step rather than the molecular binding parameters. An example for a methodology to study surface-binding kinetics that overcomes this problem is total internal reflection fluorescence correlation spectroscopy, where the kinetic information is extracted from the equilibrium fluctuations (Lieto *et al*., 2003). In SPR, the range of on-rate constants where one may observe the onset of transport limitation is at 10^5–$10^6\,M^{-1}\,s^{-1}$ (Jönsson and Malmqvist, 1992; Schuck, 1997b), but this is

strongly dependent on size, charge, and nonspecific binding of the analyte, as well as on the surface density of the immobilized sites (Karlsson, 1994; Schuck, 1996). Mass transport is a practical problem in many (or perhaps most) kinetic SPR-binding experiments (Karlsson *et al*., 1994), and if disregarded, the apparent binding parameters may be up to several orders of magnitude in error. Unfortunately, the procedure to account for mass transport initially proposed by the manufacturer (Biacore) (Karlsson *et al*., 1991) was incorrect (Glaser, 1993; Schuck and Minton, 1996). However, since then, the transport process has been well studied, and analytical and diagnostic methods have been developed.

One can examine the transport process on three different levels. First, the rate of macroscopic buffer exchange in the flow cell has been considered (Glaser, 1993; van der Merwe *et al*., 1994; Hall *et al*., 1996), which clearly provides estimates for an upper limit of the detectable rate constants. A more detailed view is possible considering the diffusion of the analyte through the laminar flow across the surface (Glaser, 1993; Karlsson *et al*., 1994; Yarmush *et al*., 1996). This predicts that the transport rate increases only with the cube root of the flow rate. Finally, an additional transport step is the diffusion through the array of binding sites within the immobilization matrix, if such a matrix is used. Even though the matrix is generally very thin (estimates for some of the commercially available surfaces range between 100 and 400 nm (Stenberg *et al*., 1991; Yeung *et al*., 1995)), it has been proposed that it may under some conditions be the rate-limiting step of transport (Schuck, 1996). According to Wofsy and Goldstein (2002), the latter requires the diffusion coefficient in the matrix to be substantially lower (one or two orders of magnitude) than that in the bulk. Such conditions may exist for highly functionalized matrices, where steric hindrance and electrostatic interactions with the charged polymer lead to restricted diffusion (Schuck, 1996). Further, nonspecific binding to the sensor surface can reduce the analyte mobility very substantially (Crank, 1975), even at a level where nonspecific binding causes signals only on the order of common bulk refractive index offsets (Schuck, 1997a). This question was addressed experimentally in studies with different model systems, where the presence of the dextran matrix did (Piehler *et al*., 1999; Fong *et al*., 2002) and did not (Karlsson and Fält, 1997; Parsons and Stockley, 1997) have an influence on the surface-binding kinetics.

A hallmark of reaction, diffusion, and convection processes in general is the formation of spatial gradients and reaction fronts. Computer simulations for the binding process in the SPR biosensor showed that under transport-limited conditions, spatial gradients within the sensing volume can form, which may generate characteristic artifacts in the measured signal due to the spatially inhomogeneous sensitivity of detection. Spatially inhomogeneous binding progress in a direction perpendicular to the surface was experimentally observed by dual-color SPR during the immobilization of streptavidin into a dextran hydrogel (Zacher and Wischerhoff, 2002). It has been proposed that spatial inhomogeneities may explain some experimentally reproducibly observed artifacts in strongly transport-limited-binding experiments, which show an increasing slope in the association phase and an increasing signal in the dissociation phase, if it follows only partial saturation of

the surface sites (Schuck, 1996). In particular, the increasing signal in the dissociation phase cannot be explained from chemical kinetics alone, without invoking spatial gradients and considering the spatially nonuniform sensitivity. Besides the obvious problem is that when transport is the rate-limiting step of binding, relatively less information on the chemical kinetics can be contained in the surface-binding traces, such effects from spatial parameters governing transport and the detection of binding considerably constrain the reliability of kinetically modeling strongly mass transport-limited surface binding (see later).

The simplest form of addressing gradients in the analyte concentration is a two-compartment model. In this highly simplified model, the transport is considered in a framework similar to chemical kinetics, as an abstract-partitioning step from a well-mixed compartment into another well-mixed compartment close to the sensor surface containing the binding sites

$$\begin{aligned}\frac{\mathrm{d}c_{\mathrm{surf}}}{\mathrm{d}t} &= k_{\mathrm{tr}}(c_{\mathrm{bulk}}-c_{\mathrm{surf}})-k_{\mathrm{on}}(b_{\mathrm{tot}}-b)c_{\mathrm{surf}}+k_{\mathrm{off}}b \\ \frac{\mathrm{d}b}{\mathrm{d}t} &= k_{\mathrm{on}}(b_{\mathrm{tot}}-b)c_{\mathrm{surf}}-k_{\mathrm{off}}b\end{aligned} \tag{4.6}$$

with c_{surf} and c_{bulk} denoting the concentration of the soluble analyte close to the surface and in the bulk, b and b_{tot} the bound analyte and the surface-binding capacity, respectively, and k_{tr} an effective transport rate constant. Even though limitations of this model are obvious, since it implies the existence of well-mixed surface and flow compartments, it can serve as a first-order approximation of transport contributions to the binding kinetics for the range of chemical binding reactions at the onset of transport limitation, that is, where the molecular on-rate constants are slow enough to make the overall surface-binding kinetics essentially reaction controlled and only slightly influenced by the transport step (Schuck and Minton, 1996).

The basic features of transport limitation are reduced rate constants of both surface binding and dissociation. Close to the surface, the capture of soluble analyte by the immobilized sites proceeds at a higher rate constant than the analyte supply from the bulk flow, such that a depletion zone is established where the soluble analyte concentration is reduced (Figure 4.3B). *Vice versa*, in the dissociation phase the rate constant of dissociation is faster than the analyte can be rinsed out, such that a zone of nonvanishing analyte concentration is maintained, which can be subjected to rebinding to the empty surface sites. In both cases, the extent of transport influence is governed by the ratio of the surface-binding flux $k_{\mathrm{on}}b_{\mathrm{free}}c$ (with b_{free} denoting the concentration of free surface sites) relative to the transport flux $k_{\mathrm{tr}}c$, that is, the transport influence is governed by the chemical on-rate constant. In the association phase, the depletion zone causes a reduction in the curvature of the surface-binding progress, which, at analyte concentrations greater than K_{D}, is distinct from the exponential binding progress expected in the absence of transport limitation. If the dissociation is started from close to saturation, relatively fewer empty surface sites are available for rebinding as compared with dissociation at lower binding levels, and the resulting time course of dissociation can be empirically fit very well

with a double exponential, where both apparent rate constants are below (and possibly far from) the true molecular off-rate constant (Figure 4.4). Unfortunately, at concentrations smaller than K_D, the transport-limited traces still closely follow single exponential shape, mimicking ideal binding at reduced rate constants.

For the onset of transport influence on the surface-binding kinetics, the two-compartment model predicts (under steady-state conditions for the free analyte close to the sensor surface) the following influence on the apparent rate constants

$$\frac{k_{on,app}}{k_{on,true}} = \frac{k_{off,app}}{k_{off,true}} = \frac{1}{1 + b_{free}(t)k_{on,true}/k_{tr}}, \tag{4.7}$$

where the subscripts app and true refer to the apparent and true on- and off-rate constants, and k_{tr} denotes the transport rate constant. Eq. (4.7) shows that the transport effect scales directly with the number of available surface sites. Therefore, limiting the immobilized density of sites is an important strategy to minimize mass

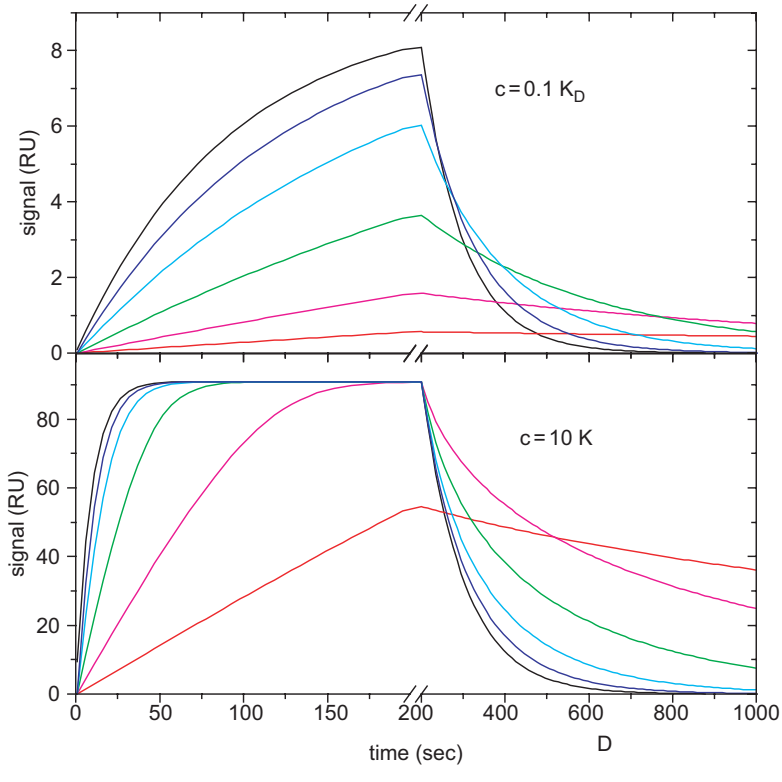

Figure 4.4. Transport-limited-binding kinetics for different analyte concentrations. Simulated with $k_{on}{}^{*}r_{max}/k_{tr} = 0$ (black), 0.33 (blue), 1 (cyan), 3.3 (green), 10 (magenta), and 33 (red). At low concentrations ($c < K_D$), traces are close to single exponentials, whereas at high concentrations ($c > K_D$) traces show a linearized association and a double exponential dissociation phase.

transport, and the variation of surface density of the immobilized sites is an excellent test for the presence of mass transport influence. In the context of a global fit of binding progress to the different surfaces, this may allow the derivation of estimates of the magnitude of k_{tr}. Another excellent qualitative test is the injection of a soluble form of the immobilized binding partner during the dissociation phase, which can serve as a competitor and prevent rebinding to the surface sites and lead to an accelerated dissociation if transport limitation is present.

4.4. STUDYING INTERACTING SYSTEMS WITH MULTIPLE COMPONENTS, BINDING SITES, OR CONFORMATIONAL STATES

Most of the fundamentals of cellular processes rely on the formation of complexes of multiple proteins, as they exceed the mechanistic limitations of simple binary binding reactions. The identification of vast networks of interacting proteins within the cell (McCraith *et al*., 2000; Uetz *et al*., 2000; Walhout *et al*., 2000; Ito *et al*., 2001; Rain *et al*., 2001; Gavin *et al*., 2002; Ho *et al*., 2002; Giot *et al*., 2003; Li *et al*., 2004) has highlighted the interdependency of many of these processes and their reliance on such multiprotein complexes. Analysis of the associations of multiple proteins will likely become only more important in the post-genomic era as focus shifts from genomes to interactomes, the networks of protein–protein interactions encoded by whole genomes. While the rules that govern the interaction between two individual proteins in forming a bimolecular complex are yet to be fully elucidated (Bogan and Thorn, 1998; Lo Conte *et al*., 1999; Sundberg and Mariuzza, 2000, 2002; Ma *et al*., 2001), the association of more than two binding partners in a single multiprotein complex introduces further levels of complexity to the binding reaction that must also be addressed.

One hallmark of multiprotein complexes is cooperativity. As the affinity of proteins for their ligands is a fundamental property that determines the dynamic range within which they operate, binding affinity either gained or lost via cooperative interactions makes important contributions to the functionality of the resulting multiprotein complex (Germain and Stefanova, 1999; Courey, 2001). To understand fully the role of cooperative binding in protein function, it is necessary to describe quantitatively each binary reaction that together comprises the multiprotein association and how each of these reactions is affected energetically by others in the overall complex. Studying the binding mechanisms of multiprotein complexes, however, is complicated by the intricacy of the reaction schemes, as well as the need for structural information and highly homogeneous sources of purified protein. While the rate at which atomic structures of multiprotein complexes are described continues to increase, the energetic analysis of these higher-order molecular interactions, in which cooperativity is likely to be a frequent attribute, has lagged well behind.

When studying systems of more than two binding partners or with multiple sites or conformational states, a variety of experimental configurations are possible

in the SPR biosensor. To illustrate the potential of the technique, we consider three systems: (1) binding of A and B where A can undergo a conformational change to A^*; (2) a molecule A with multiple binding sites for B; and (3) a molecule A that has separate sites for two molecules B and C.

4.4.1. Multiple Conformational States

Several authors have considered the presence of different conformational states and binding-induced conformational changes in the interaction proteins, including quantitative studies of antibody–antigen interactions (Glaser and Hausdorf, 1996; Lipschultz *et al*., 2000) and other protein–protein interactions (De Crescenzo *et al*., 2000; Honjo *et al*., 2002; Khursigara *et al*., 2005), as well as mapping of binding-induced conformational changes in proteins with conformationally specific antibodies (e.g., Dubs *et al*., 1992; Cohen *et al*., 1995; Fischer *et al*., 1996).

For the reactions $A \overset{K_C}{\longleftrightarrow} A^*$, $A+B \overset{K}{\longleftrightarrow} (AB)$, and $A^*+B \overset{K^*}{\longleftrightarrow} (AB)^*$, let us denote K_C as the equilibrium constant for the conformational transition, and K and K^* the equilibrium constants for the formation of the complexes (AB) and $(AB)^*$, respectively. Since the SPR signal is proportional to the mass and refractive index increment, and in practice essentially insensitive to conformations (sensitivity to conformation is possible with waveguide sensors that use two evanescent fields with different polarization and decay length, thus obtaining more information on the geometric orientation of the protein at the surface (Salamon *et al*., 1999; Alves *et al*., 2004)), the experimentally measured surface-bound complex is $([ab]+[ab]^*)$ (with the lower case letters denoting species concentrations). The mass action law for the formation of the experimentally measurable complex $([ab]+[ab]^*)$ from $(a+a^*)$ and b follows an equilibrium constant $K_{app} = K(1 + K_C K^*/K)(1 + K_C)$; thus, not surprisingly, it cannot be inferred from an equilibrium experiment that we have different conformations of A, or if there is preferential binding of B to either one.

This situation is different in kinetic experiments, if the protein with the multiple conformational states is immobilized to the sensor surface (here one assumes that the immobilization procedure does not affect the ability of the protein to adopt the entire range of conformations that it does in solution). In this case, binding progress follows the rate equations

$$\begin{aligned}
\frac{da}{dt} &= -k_{f,a}a + k_{r,a}a^* - k_{on}ab + k_{off}c \\
\frac{da^*}{dt} &= +k_{f,a}a - k_{r,a}a^* - k^*_{on}a^*b + k^*_{off}c^* \\
\frac{dc}{dt} &= -k_{f,c}c + k_{r,c}c^* + k_{on}ab - k_{off}c \\
\frac{dc^*}{dt} &= +k_{f,c}c - k_{r,c}c^* + k^*_{on}a^*b - k^*_{off}c^* \\
S(t) &\sim c(t) + c^*(t)
\end{aligned} \tag{4.8}$$

with a and c denoting the surface concentration of the free surface-immobilized protein and the complex, respectively, b the concentration of the soluble analyte, the asterisk referring to the alternate conformation, $k_{f,a}$ and $k_{r,a}$ denoting the forward and the reverse rate constants for conformational transition of the unliganded molecule A, and the subscript a and c indicating the analogous rate constants for conformational change of the free molecules and the complex, respectively. The most interesting feature of this situation occurs if the two conformations result in different complex stabilities, as illustrated in Figure 4.5. Initial rapid binding to the low-affinity (high k_{off}) sites is followed by continuous conversion of the low affinity with the more slowly dissociating (generally high-affinity) sites (Figure 4.5, red and magenta lines). This introduces a history dependence of the dissociation process, which is indicative of more complex interactions. At an equivalent binding level, the dissociation is slower for configurations with longer contact times preceding the dissociation (providing more time for conversion of the sites). Such a history dependence cannot be explained by the existence of multiple independent classes of surface sites. The analysis of binding with conformational changes is reviewed by Lipschultz *et al*. (2000).

Unfortunately, this history-dependent behavior is not unique to systems with conformational changes. Very similar curves are observed for binding to a single class of surface sites, if the analyte is heterogeneous and consists of multiple, competitively binding species with different binding properties (circles in Figure 4.5) (Svitel *et al*., 2003). This situation may arise if the soluble protein exists in different conformations with different binding properties (in the flow system, the time which the analyte spends close to the sensor surface is typically too short to allow conformational transitions of the soluble analyte to be relevant before it is being replenished). Alternatively, the analyte may exist in mixtures of monomeric and multimeric forms that differ in their binding properties, for example, due to avidity effects (see earlier).

It can be difficult to distinguish between these cases on the basis of the SPR-binding data alone. This has generally been observed for models with complex kinetic-binding schemes (Glaser and Hausdorf, 1996; Karlsson and Fält, 1997; Schuck, 1997a; De Crescenzo *et al*., 2000). This is rooted in the well-known problems of fitting noisy exponentials, reminiscent of data analysis problems in many other biophysical disciplines, some of which are illustrated in other chapters. The ambiguity can be resolved, however, if independent information is available from other biophysical methods that can report on conformational changes. For example, De Crescenzo and colleagues (2000) discuss the consistency of the conformational change model for the interaction of transforming growth factor α with epidermal growth factor receptor extracellular domain with the results from circular dichroism (Greenfield *et al*., 1989). Other techniques to study conformational changes upon binding are described in other chapters, including hydrodynamic, spectroscopic, and mass spectrometry approaches.

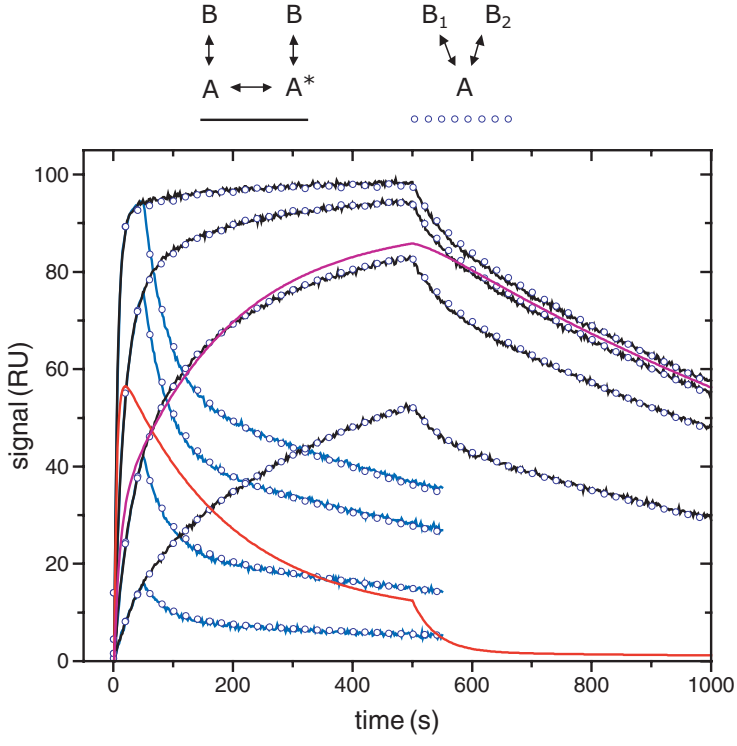

Figure 4.5. Illustration of surface-binding kinetics with surface sites undergoing a conformational change. Binding curves are simulated for a low-affinity conformation ($K_{D,1} = 100\,\text{nM}$, $k_{dis,1} = 2 \times 10^{-2}\ \text{s}^{-1}$) and a high-affinity conformation ($K_{D,2} = 5\,\text{nM}$, $k_{dis,2} = 5 \times 10^{-4}\ \text{s}^{-1}$) with slow conformational transition ($k_{cf,12} = 1 \times 10^{-2}\ \text{s}^{-1}$) and with initially two-thirds of the unliganded surface sites in the low-affinity state, and with a shift of the conformational equilibrium toward the high-affinity site due to stabilization by the ligand (tenfold excess of high-affinity sites in equilibrium). Surface-binding curves are for soluble analyte concentrations of 30, 100, 300, and 1,000 nM, for 50 and 500 s contact time (solid blue and black lines, respectively). It should be noted that the dissociation after long contact times is much slower than that after short contact times. This is due to the slow conformational transition of the bound and the free surface sites. For illustration, the conversion of the complex with low affinity into high-affinity conformation is indicated for the highest analyte concentration by solid red and magenta lines, respectively. The dependence of the off rate on the contact time is qualitatively incompatible with the existence of multiple conformationally stable surface sites. However, very similar binding progress can be obtained for single, stable surface sites, if the analyte is heterogeneous in its binding properties. In this case, lower-affinity analyte is replaced during the contact time by higher-affinity, slower dissociating analyte. The best-fit traces for a mixture of two analytes binding competitively to the same surface site are indicated as circles. In the case shown, the binding is calculated for a low-affinity analyte with $K_{D,1} = 133\,\text{nM}$ and $k_{dis,1} = 2.2 \times 10^{-2}\ \text{s}^{-1}$ and a high-affinity analyte with $K_{D,2} = 7\,\text{nM}$, $k_{diss,2} = 9.5 \times 10^{-4}\ \text{s}^{-1}$, with the second site at a constant 46% of the total analyte concentration. The root-mean-square (rms) deviation between the model of two surface sites with conformational equilibrium and the model of competitively binding analyte mixtures is 0.7 RU, which is experimentally virtually indistinguishable.

4.4.2. Multiple Binding Sites

The second system we consider is a soluble protein B binding to multiple independent surface sites $A_1, A_2, \ldots A_n$, each with different binding properties. This model can describe binding to a surface-immobilized protein with different, independent epitopes, binding to an intrinsically heterogeneous ensemble of proteins at the surface (e.g., due to sequence variability or variation in glycosylation), or it may be used to account for partially inactivated sites from surface immobilization or from constraints imposed by heterogeneity in the microenvironment of the surface sites. Frequently, the number of existing classes of surface sites may not be known *a priori*, or the binding properties may vary quasicontinuously for different subclasses of sites. A useful approach is the description of the surface sites as a continuous distribution $c(k_{\mathrm{off}}, K_{\mathrm{D}})$, where the differential $c(k_{\mathrm{off}}, K_{\mathrm{D}})\mathrm{d}k_{\mathrm{off}}\,\mathrm{d}K_{\mathrm{D}}$ is the surface concentration of sites with off-rate constants between k_{off} and $k_{\mathrm{off}} + \mathrm{d}k_{\mathrm{off}}$ and with equilibrium constant between K_{D} and $K_{\mathrm{D}} + \mathrm{d}K_{\mathrm{D}}$ (Svitel *et al.*, 2003). The experimentally measured kinetic-binding curves can be modeled as

$$S(b,t) \cong \int_{K_{\mathrm{D,min}}}^{K_{\mathrm{D,max}}} \int_{k_{\mathrm{off,min}}}^{k_{\mathrm{off,max}}} c(k_{\mathrm{off}}, K_{\mathrm{D}})\, s\,(k_{\mathrm{off}}, K_{\mathrm{D}}, b, t)\, \mathrm{d}k_{\mathrm{off}}\, \mathrm{d}K_{\mathrm{D}}, \tag{4.9}$$

where $S(b, t)$ are binding signals at times t and concentrations of soluble analyte b, and with $s(k_{\mathrm{off}}, K_{\mathrm{D}}, b, t)$ denoting the standard pseudo first-order binding kinetics Eqs (4.2–4.4). Equation (4.9) can be modified with a compartment-like transport step to account for the binding kinetics at the onset of transport-limited binding (Svitel *et al.*, submitted). This represents a data transformation from the space of surface-binding signals to a space of binding constants, reminiscent to a Laplace transform of exponentials. Although the numerical solution of Eq. (4.9) is unstable for high discretization of k_{off} and K_{D}, it can be combined with maximum entropy or Tikhonov regularization approaches that will determine the simplest distribution consistent with the experimental data (at the given signal and noise level) (Hansen, 1998). This regularization strategy has been introduced by Provencher (1982) very successfully to the analysis of dynamic light-scattering data in the software CONTIN. The approach in Eq. (4.9) is similar to the concept of using sedimentation coefficient distributions $c(s)$ in analytical ultracentrifugation (Schuck, 2000) to account for all sedimentable material (chapter 16). Likewise, the surface site distribution allows experimental imperfections, such as arising from immobilization, baseline drifts and nonspecific binding, as well as multiexponential binding from many specific sites, to be transformed from the original data space into the space of binding constants, where they can be identified and excluded from further consideration, without biasing or oversimplifying the analysis of the sites of interest.

Figure 4.6 shows the application to different antibody–antigen interactions, and illustrates the gain in quality of fit if the heterogeneity of the surface sites is

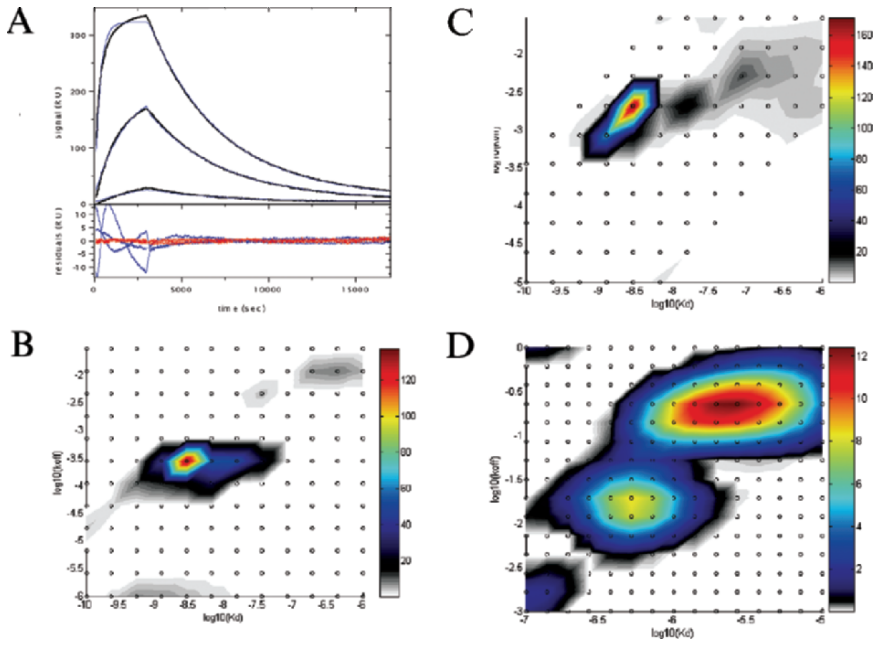

Figure 4.6. Distributions of surface sites calculated from families of experimental kinetic-binding curves. (A) (*top*) Binding traces for the antigen B5R (0.5, 5, and 50 nM) binding to antibody 19C2 (Schmelz *et al*., 1994) (a kind gift from Dr Berhard Moss), immobilized on a long-chain carboxymethyl dextran (Biacore CM5) (Chen *et al*., 2006). Experimental traces (black) and best-fit assuming a single site model (blue lines). (A) (*bottom*) Residuals of the fit with a single site model (blue lines, rms deviation (rmsd) = 3.4 RU) and with the distribution model (red lines, rmsd = 0.43 RU). (B) Distribution reveals a low level of heterogeneity, indicating a small subpopulation of slightly lower-affinity sites over a narrow K_D range. The circles indicate the gridpoints for the numerical solution of Eq. (4.9). (C) Distribution of surface sites for transport-limited binding of β_2-microglobulin to an immobilized monoclonal antibody (Svitel *et al*., submitted). (D) The distribution of sites for binding of a soluble Fab fragment of a variant of mAb CC49 to immobilized bovine mucin (Svitel *et al*., 2003). The CC49 antibody recognizes the tumor-associated glycoprotein TAG-72 via epitopes. They are the trisaccharide Galβ(1–3)[NeuAcα(2–6)]GalNAc and the disaccharide structure [NeuNAcα(2–6)]GalNAc, linked to serine or threonine side chains (Hanisch *et al*., 1989). Both the disaccharide and the trisaccharide structures are also present in bovine and ovine submaxillary mucins (Reddish *et al*., 1997). Therefore, the interaction of the Fab with immobilized mucin is an example where intrinsically multiple classes of ligand are present. Accordingly, the two main peaks of the distribution have been attributed to the trisaccharide and the disaccharide structures.

accounted for. This model has been applied, for example, in a study of the ligand recognition of $\alpha_x\beta_2$ integrin (Vorup-Jensen *et al*., 2005), and in the characterization of antibody–antigen interactions (Chen *et al*., submitted). An analogous (one-dimensional) distribution of affinity constants can be applied to the isotherm analysis of steady-state binding data, as applied to the analysis of anthrax toxin residues interacting with the neutralizing antibody (Rosovitz *et al*., 2003).

4.4.3. Trimolecular Interactions

Perhaps the most interesting system in the present context is a ternary interaction of protein A binding two proteins B and C on separate sites, forming complexes [AB], [AC], and [ABC]. If A is immobilized to the sensor surface, binding can be probed with B, C, and mixtures of B and C. Mutual interactions of B and C may be detected through deviations of the binding signal of the mixture from being a linear superposition of the predetermined binding curves of B and C alone. The steady-state binding signal S as a function of solution concentrations b and c follows the isotherm

$$S(b, c) = \frac{s_{\mathrm{A,active}}}{M_{\mathrm{A}}} \frac{M_{\mathrm{B}} b K_{\mathrm{AB}} + M_{\mathrm{C}} c K_{\mathrm{AC}} + (M_{\mathrm{B}} + M_{\mathrm{C}}) ab\ \alpha K_{\mathrm{AB}} K_{\mathrm{AC}}}{1 + b K_{\mathrm{AB}} + c K_{\mathrm{AC}} + ab\ \alpha K_{\mathrm{AB}} K_{\mathrm{AC}}} \tag{4.10}$$

with $s_{\mathrm{A,active}}$ denoting the surface concentration, in signal units, of the active fraction of the immobilized species A, and the factors M_{A}, M_{B}, and M_{C} are the molecular weights accounting for the signal contributions due to the different size of the binding partners (a further correction should be applied for differences in refractive index of the components). The constant α indicates positive ($\alpha > 1$) or negative ($0 < \alpha < 1$) cooperativity.

Figure 4.7 shows binding isotherms expected for the steady-state signal of equimolar mixtures of B and C. For positive cooperativity, the isotherm becomes slightly steeper and exhibits a midpoint at significantly lower concentrations than the K_{D} (for simplicity, it is assumed in this illustration that $K_{\mathrm{AB}} = K_{\mathrm{AC}}$, but similar conclusions can be drawn in the general case). In contrast, in the presence of negative cooperativity, the binding at low concentration is less affected since both molecules B and C can bind to different molecules of A available at the surface. However, the isotherm becomes broader and biphasic, as it requires much higher concentrations to exceed half-saturation of the surface sites.

In some regard, the possibility at lower concentration of parallel binding to different surface sites may represent a practical limitation of this configuration. Therefore, we next consider an arrangement where B is immobilized to the surface, and both A and C are soluble. If C does not interact with B, it can bind to the surface only via A as a bridge. If we assume that A and C are applied to the sensor surface as an equilibrium mixture, the concentrations of free A and of the complex [AC] in solution can be calculated from the solution interaction isotherm [Eq. (4.5)], and the total surface-binding isotherm then follows

$$S(a_{\mathrm{tot}}, c_{\mathrm{tot}}) = \frac{s_{\mathrm{B,active}}}{M_{\mathrm{B}}} \frac{M_{\mathrm{A}} K_{\mathrm{AB}} a_{\mathrm{free}} + (M_{\mathrm{A}} + M_{\mathrm{C}}) \alpha K_{\mathrm{AB}} [\mathrm{AC}]}{1 + K_{\mathrm{AB}} a_{\mathrm{free}} + \alpha K_{\mathrm{AB}} [\mathrm{AC}]}. \tag{4.11}$$

The steady-state surface-binding signal dependent on the total concentrations of A and C exhibits several characteristic features (Figure 4.8). First, at any given concentration of A, the coinjection with C to form soluble complex [AB] that can bind to the surface will increase the signal, as reflected by the lines in Figure 4.8A at

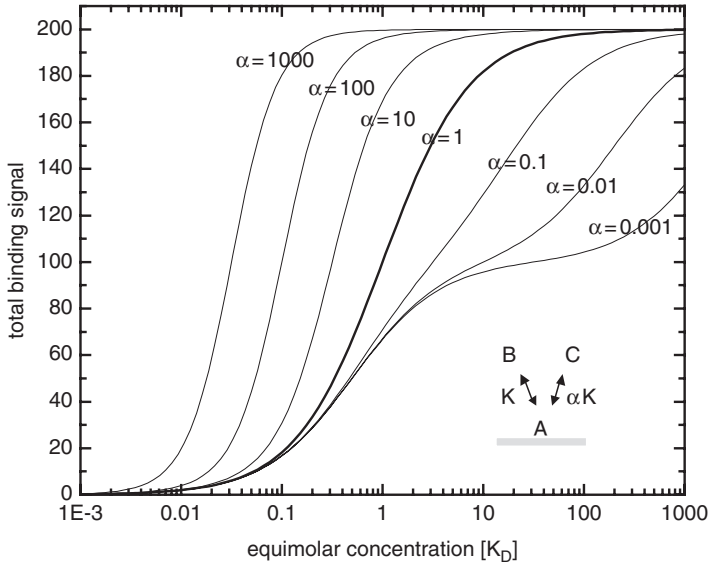

Figure 4.7. Steady-state binding curves for two soluble ligands B and C binding to the same surface-immobilized protein A, with different cooperativity factors α in Eq. (4.10). It is assumed that B and C are in equimolar concentration, have the same signal contribution, and that both have the same binding constant to A ($K_{AB} = K_{AC}$).

constant a_{tot} and varying c_{tot}. Interestingly, the perpendicular lines, showing the signal for a given concentration of soluble ligand c_{tot} and varying concentration a_{tot} will exhibit a maximum. This occurs because as we are increasing the molar excess of A over C, free A will increasingly compete with [AC] for the available surface-binding sites, and due to the smaller mass of A compared with [AC], this will result in a decrease of the measured signal. The effect of cooperativity is that of modulating the affinity of [AC] to the surface relative to free A. Positive cooperativity will lead to a stronger enhancement of surface binding, for example, visible in the higher slope of lines at constant a_{tot} and increasing c_{tot} (Figure 4.8B). For negative cooperativity, the same lines of constant a_{tot} can exhibit a qualitatively different feature, in the form of a negative slope (Figure 4.8C). This is due to competition for A between soluble C and surface-immobilized B, and can be clearly visible even at relative low concentrations of A. An application of this model will be described later for the study of ternary interactions of a bacterial SAG, MHC molecules, and TCR fragments (see Section 4.4). For the cooperative multistep association of RANTES with heparin, a related, but more complex, binding scheme was proposed by Vivès *et al.* (2002), which was described with a model for the equilibrium isotherm binding.

This approach of the coinjection of mixtures of soluble molecules is suitable also for kinetic experiments. Examples are the kinetic study of the ternary

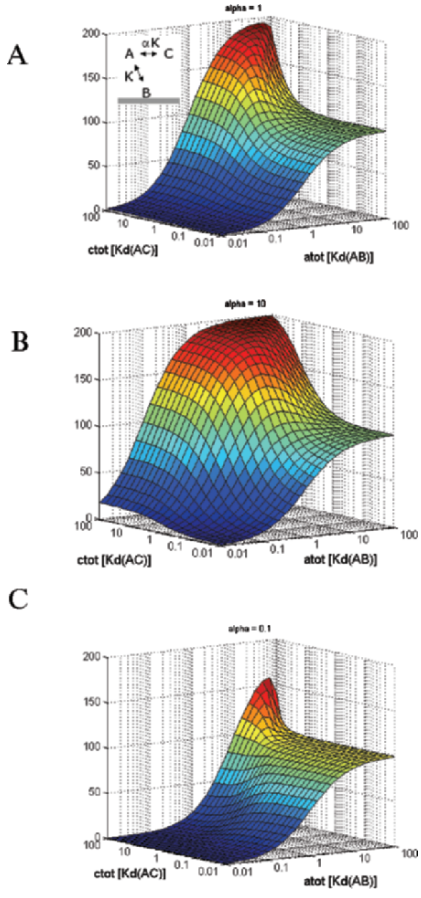

Figure 4.8. Steady-state surface-binding isotherms for two interacting soluble proteins A and C, which can form a reversible soluble complex [AC], binding to the surface-immobilized protein B forming surface-bound complexes [AB] and [ABC]. The effect of different cooperativity factors α from Eq. (4.11) is shown. It is assumed that A and C have the same signal contributions. The total soluble concentrations of A and C are expressed in units of the equilibrium dissociation constants. The cooperativity factors are 1 (A), 10 (B) and 0.1 (C), respectively.

interaction of TCR, MHC class II, and SAG SEA (Redpath *et al*., 1999) in the interaction of fibroblast growth factor, its receptor, and heparin (Ibrahimi *et al*., 2004), and the interactions of insulin-like growth factor-binding proteins (Beattie *et al*., 2005).

For systems with suitably slow dissociation, the kinetic experiments allow for an even more direct visualization of the second binding site for A, if sequential injections of A and C are used, such that C comes in contact only with the preformed surface-bound complex AB (Figure 4.9). This configuration exploits the ability of the flow system to separate soluble A from the complex captured

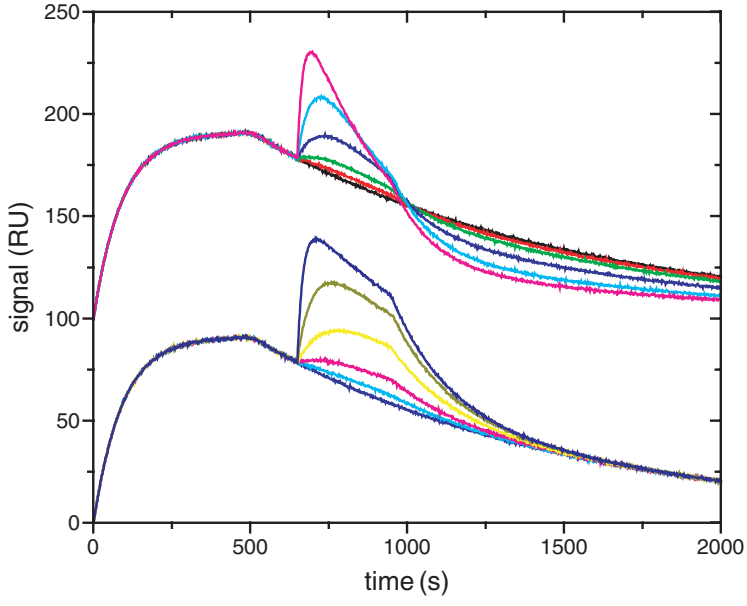

Figure 4.9. Examples of kinetic traces of triple protein interactions. Simulated binding curves of a soluble protein A binding to surface-immobilized surface sites B, followed by binding of protein C to the preformed surface-bound complex [AB]. Binding curves are calculated for binding of A with an equilibrium constant $K_{D,AB} = 10\,\text{nM}$, an off-rate constant of $k_{off,AB} = 1 \times 10^{-3}\ \text{s}^{-1}$, and with maximal capacity of 100 RU units. Contact time of A with the surface-immobilized B is 500 s. After 200 s of dissociation in a buffer wash, protein C is introduced into the flow for 300 s at concentrations of 10 (red), 30 (green), 100 (blue), 300 (cyan), or 1,000 nM (magenta), followed by rinsing with buffer. C is assumed to have the same mass as A, resulting in the same signal contribution. Binding of C to preformed [AB] proceeds with $K_{D,C[AB]} = 100\,\text{nM}$ and $k_{off,AB} = 5 \times 10^{-3}\ \text{s}^{-1}$. For reference, the undisturbed dissociation of A without introduction of C is indicated by the black line. The lower curves assume no cooperativity of C on the interaction of A–B. In contrast, the upper curves (offset by 100 for clarity) illustrate the case where C destabilizes the interaction of A–B, with a threefold enhancement of dissociation [CA]–B over A–B.

at the sensor surface. Since the complex will continuously dissociate, these experiments can generally only be conducted in conjunction with a global kinetic analysis of the binding curves. The rate equations during the dissociation follow

$$\begin{aligned}\frac{\mathrm{d}(ab)}{\mathrm{d}t} &= -k_{\text{off,a}}(ab) - k_{\text{on,C}}(ab)c_{\text{sol}} + k_{\text{off,C}}(abc)\\ \frac{\mathrm{d}(abc)}{\mathrm{d}t} &= k_{\text{on,C}}(ab)c_{\text{sol}} - (k_{\text{off,AC}} + k_{\text{off,C}})(abc)\\ S(t) &\sim M_{\text{A}}(ab)(t) + (M_{\text{A}} + M_{\text{B}})(abc)(t)\end{aligned} \tag{4.12}$$

with *ab* and *abc* denoting the surface concentrations of the complexes [AB] and [ABC], respectively, c_{sol} the solution concentration of C, $k_{\text{off},a}$ the off-rate constant

of A from B, $k_{on,C}$ and $k_{off,C}$ the on- and off-rate constants of C binding to A, and $k_{off,AC}$ the off-rate constant of the complex [AC] dissociating from B. Families of curves with different c_{sol} are shown in Figure 4.9. If binding of C to the preformed complex [AB] destabilizes the interface of A and B, a characteristic acceleration of overall surface dissociation may be discerned. This can be taken as a qualitative sign for such a destabilizing effect of C. As with the experimental configurations described earlier for studying this system, it cannot be deduced from the data in Figure 4.9 if the observed cooperativity between the ligands B and C stems from conformational changes propagated through A, or from the proximity of B and C on A leading to repulsive or attractive interactions between the two ligands. As will be shown later, this question may be addressed with control experiments analyzing interactions of B and C, and in combination with a structural technique. In addition, circular dichroism can be useful to detect conformational changes in the triple complex (Arthos *et al*., manuscript in preparation).

The kinetic analysis in this configuration is described in more detail by Joss *et al*. (1998). It has been applied, for example, by Walsh *et al*. (2003) to the study of human growth hormone (hGH) receptor–ligand interactions. hGH forms a 1:2 ligand–receptor complex involving two distinct receptor sites. In this study, the extracellular domain containing site 1 of the receptor was immobilized on a dextran matrix, saturated with soluble hGH, and the binding kinetics of soluble receptor with the preformed 1:1 complex was studied. Alanine mutations in hGH site 2 were inserted to study the role of side chains contributing to the overall binding energy of site 2 and the cooperativity of their contributions (Walsh *et al*., 2003). In a different configuration, Bernat *et al*. (2003) employed a dextran-free carboxylated surface for the immobilization of the hGH receptor, such that no lateral receptor interactions are permitted and upon saturation with hGH only hGH/receptors site 1 complexes can be formed, which, in turn, can capture soluble receptor to form the 1:2 complex, making the latter reaction accessible for study.

Sequential binding studies can be carried out with systems of greater complexity than those discussed so far. For example, Schuster *et al*. (1993) have exploited a configuration of sequential injection of proteins participating in a quaternary chemotactic signal transduction complex. For qualitative information, even higher-order multiprotein complexes have been studied by sequential binding of soluble ligands, such as the DNA polymerase III holoenzyme complexes (Dallmann and McHenry, 1995) and multi-antibody–antigen complexes in context of antibody epitope mapping (Fägerstam *et al*., 1990).

For the study of trimolecular interactions, a third experimental configuration is possible; the coupling of two different molecules to the same surface (in the terminology used earlier, it would represent the surface immobilization of both B and C, to probe the reversible interaction of soluble A). This seems attractive when studying interactions with multiple copies of cell-surface receptor molecules. However, when using a polymeric immobilization matrix, a possible concern for the quantitative interpretation of binding in this orientation appears to be the unknown relative mobility of the immobilized molecules within the matrix and the possibility

of energetic constraints from the microenvironment influencing their ability to interact with each other.

In different situations, this approach has been applied in the literature to study receptor–ligand interactions (Cunningham and Wells, 1993; Myszka *et al*., 1996; Stokes *et al*., 2005). In the study of hGH receptor–ligand interactions, Cunningham and Wells (1993) established that by introducing mutations in different residues of the receptor, the mode of soluble ligand binding to immobilized receptor could be controlled, allowing either only 1:1 complexes via site 1 of the receptor, or the formation of ligand-induced receptor dimerization via both sites 1 and 2. This demonstrated sufficient mobility of the immobilized hGH receptor in the dextran matrix to permit formation of ternary complexes. Changes in the binding properties induced by a series of alanine mutations of residues involved in site 1 binding of hGH were measured and the relative rate constants for formation of the 1:1 complex determined, which revealed the energetic contributions of the hGH side chains to the overall binding energy of the binary complex of site 1. A quantitative interpretation of ternary ligand–receptor interactions involving mixed receptor surfaces was attempted by Myszka *et al*. (1996). Both α and β subunits of the interleukin-2 (IL-2) receptor were sequentially immobilized, and binding of soluble IL-2 was observed. Slightly faster surface binding and significantly slower dissociation was measured for the mixed surface compared with the surfaces with each of the individual receptor subunits immobilized alone. However, the binding kinetics was obscured by strong mass transport limitation, and for the reasons outlined earlier, it is an open question how much the immobilization of two subunits into the dextran matrix would affect the energetics for triple complex formation (Myszka *et al*., 1996). In a different system, Stokes *et al*. (2005) created mixed surfaces containing meningococcal transferrin-binding proteins A and B, integral membrane proteins of the outer membrane, using supported dimyristoyl phosphatidylcholine (DMPC) monolayers in the absence of a dextran matrix. Human transferrin binding to the mixed surface was more stable than binding to surfaces containing either one of the receptors alone (Stokes *et al*., 2005). A powerful approach for studying receptor subunits attached to supported lipid bilayers, the interactions in the plane of the membrane, and their role in ligand binding was developed by Piehler (see Chapter 3).

The above-mentioned three cases may serve as examples for the experimental configurations that can be encountered in the analysis of complex interacting systems with SPR biosensing. Extensions to more complex systems may be possible, although it should be noted that the information content from SPR-binding traces is frequently limited due to the problem that the experimentally measured exponential kinetic-binding curves and sigmoid steady-state isotherms may be fitted equally well with many different models. Further, more complex models can be significantly more susceptible to experimental imperfections in the sample purity, aggregation state, and detection. SPR shares these difficulties with many other techniques. Therefore, it is frequently crucial to combine the SPR data with other complementary techniques to alleviate the problem of amibuity in the modeling.

4.5. A PRACTICAL APPLICATION TO THE STUDY OF MULTIPROTEIN COMPLEXES

Instead of compiling a comprehensive literature review, we will highlight in the following the potential of SPR biosensing for the quantitative analysis of the thermodynamics of ternary complex formation by providing a more in-depth description of the application of SPR biosensing to the simultaneous interaction of a SAG with MHC and TCR molecules. This interaction exhibits both positive and negative cooperativity, and the interpretation of the SPR data is aided by the availability of structural models derived from X-ray crystallographic studies. It is likely that similar analyses are possible for other ternary interactions.

4.5.1. Superantigen–Major Histocompatibility Complex–T-Cell Receptor Interactions

SAGs are immunostimulatory and disease-associated proteins of bacterial or viral origin that bind simultaneously to class II MHC and TCR molecules on the surfaces of antigen-presenting cells and T lymphocytes, respectively (Figure 4.10A) (Sundberg *et al*., 2002). Contrary to the presentation of processed antigenic peptides by MHC to TCR, SAGs bind to MHC molecules outside of the peptide-binding groove and interact with TCR Vβ domains, resulting in the stimulation of a large fraction (up to 5–20%) of the T-cell population. In this way, SAGs are able to circumvent the normal mechanism of T-cell activation associated with antigenic peptide–MHC complexes, leading not only to massive T-lymphocyte proliferation, but also T-cell anergy and death. Accordingly, SAGs have been implicated in the pathogenesis of a number of human diseases, including toxic shock syndrome (Bohach *et al*., 1990), food poisoning (Kotzin *et al*., 1993), and several autoimmune disorders (Renno and Acha-Orbea, 1996), and are classified as bioterror reagents.

We studied the bacterial SAG, *Staphylococcus* enterotoxin C3 (SEC3), in complex with the human MHC class II molecules human lymphocyte antigen (HLA)-DR1 and a murine TCR (Andersen *et al*., 2002). In this system, the MHC molecule and the TCR do not form a specific binary complex in the absence of SEC3. Structures of each of the relevant binary complexes that comprise the MHC–SEC3–TCR ternary complex, including the SEC3–MHC class II (Sundberg *et al*., 2003), αβTCR heterodimer (Garcia *et al*., 1996), and SEC3–TCRβ-chain (Fields *et al*., 1996) complexes, have made it possible to assemble a trimolecular structural model. As shown in Figure 4.10A, this model predicts that the complex is stabilized through three distinct interfaces: SEC3–MHCα subunit, SEC3–TCRβ-chain, and TCRα-chain–MHCβ subunit.

The direct MHC–TCR interaction in this supramolecular complex has been verified by biochemical studies (Andersen *et al*., 1999). The binding energy derived from the direct contacts between the TCR and the MHC is accounted for in terms of cooperativity in the triple complex, since these molecules would not interact in the

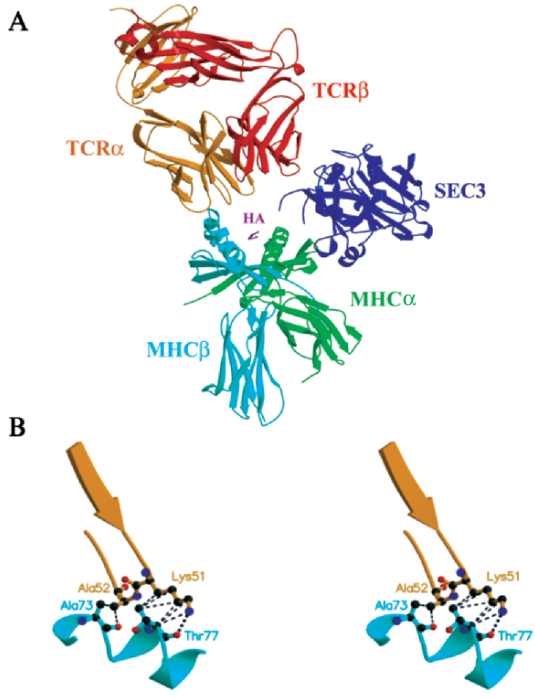

Figure 4.10. Structural model of the T-cell receptor–*Staphylococcus* enterotoxin C3–DR1 (TCR–SEC3–DR1) complex. (A) Model of the major histocompatibility complex–SEC3–TCRαβ (MHC–SEC3–TCRαβ) heterodimer complex produced by superimposing the human lymphocyte antigen–DR1–SEC3 (HLA–DR1 (HA 306–318)–SEC3) complex (Andersen *et al*., 2002), the SEC3–14.3.d TCRβ-chain complex (Fields *et al*., 1996), and the 2C TCRαβ heterodimer complex (Garcia *et al*., 1996). Overlapping SEC3 and TCRβ molecules have been removed for clarity. Colors are as follows: SEC3, blue; MHCα subunit, green; MHCβ subunit, cyan; HA (306–318) antigenic peptide, magenta; TCRα-chain, orange; and TCRβ-chain, red. (B) Molecular modeling of the DR1β subunit–TCRα-chain interface. Interactions between residues Lys51 and Ala52 from the CDR2 loop of the Vα and residues Ala73 and Thr77 from the DR1β subunit. Van der Waals interactions are indicated by dashed lines and a potential hydrogen bond between the N^{ζ} atom of Lys51 and the main chain carbonyl O of Thr77 is indicated by a dotted line. Intermolecular contacts were defined by atomic pair distances (in Å) less than or equal to the following: C–C, 4.1; C–N, 3.8; C–O, 3.7; N–N, 3.4; N–O, 3.4; O–O, 3.3. Colors are as follows: MHCβ subunit, cyan; TCRα-chain, orange; carbon atoms, black; nitrogen atoms, blue; and oxygen atoms, red. Reproduced from Andersen *et al*. (2002) with permission.

absence of SEC3. Molecular modeling of this binding site (Figure 4.10B) indicates a relatively small protein–protein interface (with a buried surface area of only ~ 400 Å^2) consisting of numerous Van der Waals interactions and a single hydrogen bond. To assess the cooperative energetics involved in the formation of the ternary complex, the contribution of the TCRα-chain–MHCβ subunit contacts must be assessed directly by comparing trimolecular complex formation in both the presence and the absence of the TCRα-chain. This is possible with this system because

biochemical and crystallographic studies have demonstrated that the isolated TCRβ-chain can interact functionally with SEC3 (Gascoigne and Ames, 1991; Malchiodi *et al*., 1995; Fields *et al*., 1996).

Figure 4.11E and F shows the response of a fixed concentration of soluble SEC3 binding to immobilized αβTCR heterodimer and the TCRβ-chain, respectively, in the presence of increasing concentrations of MHC. It is evident that increasing concentrations of MHC caused increasing accumulation of mass in the TCRαβ-coupled surface (Figure 4.11E), consistent with the binding of preformed SEC3–MHC complexes to the TCR (note that without SEC3, MHC does not bind TCR). In addition, the kinetics became significant slower, indicating enhanced stability of the trimolecular complex. In contrast, the TCRβ-chain-coupled surface responded with a lower signal when the concentration of MHC was increased (Figure 4.11F). This demonstrates that SEC3–MHC complexes have lower affinity to the TCRβ-chain than does SEC3 alone, representing negative cooperativity.

As with all SPR analyses, the experimental approach is necessarily system specific. This is especially true when studying ternary complexes. In principle, several different approaches could have been taken for analyzing the MHC–SEC3–TCR interaction (Figure 4.11A–D). Due to the relative immobilization capacities and solubilities of the constituent molecules in the supramolecular complex, the experimental design possibilities were, in reality, limited. The MHC molecule consists of three noncovalently associated polypeptides and is characterized by a relatively low isoelectric point, and thus, is intolerant to the chemical procedures necessary for amine coupling to the biosensor surface. This excluded the experimental setup depicted in Figure 4.11B. The SEC3 molecule, in contrast, is very stable and has a neutral p*I*, and therefore is not restricted in its immobilization. Thus, the experimental setup of Figure 4.11A could be used. The full-length TCR, expressed as a soluble αβ heterodimer in insect cells, had a strong tendency to aggregate. Thus, only few measurements could be made with soluble TCR immediately after size-exclusion chromatography purification, as it would not remain stable throughout the data collection period (24–48 h at ambient temperature). The αβTCR heterodimer could be immobilized (Figure 4.11C). Furthermore, it was also possible to immobilize the TCRβ-chain alone in a functional state, thereby allowing for direct comparison of complex formation in the absence of presence of the cooperative binding site on the TCRα-chain (Figure 4.11D).

Initially, each of the relevant bimolecular interactions was analyzed. The binding of SEC3 to surface-immobilized αβTCR heterodimer was evaluated by injecting increasing concentrations of SEC3 (Figure 4.12, lower insert). For the MHC–SEC3 interaction, the binding constant in solution was determined by a solution competition assay. First, SEC3 was immobilized and serial dilutions of MHC were applied to yield the K_D to the immobilized SEC3 (Figure 4.12, upper insert, in blue). Second, the binding between SEC3 and MHC in solution was determined by mixing a constant DR1 concentration with serial dilutions of SEC3 and passing these mixtures over a SEC3-coupled surface. The solution K_D was then

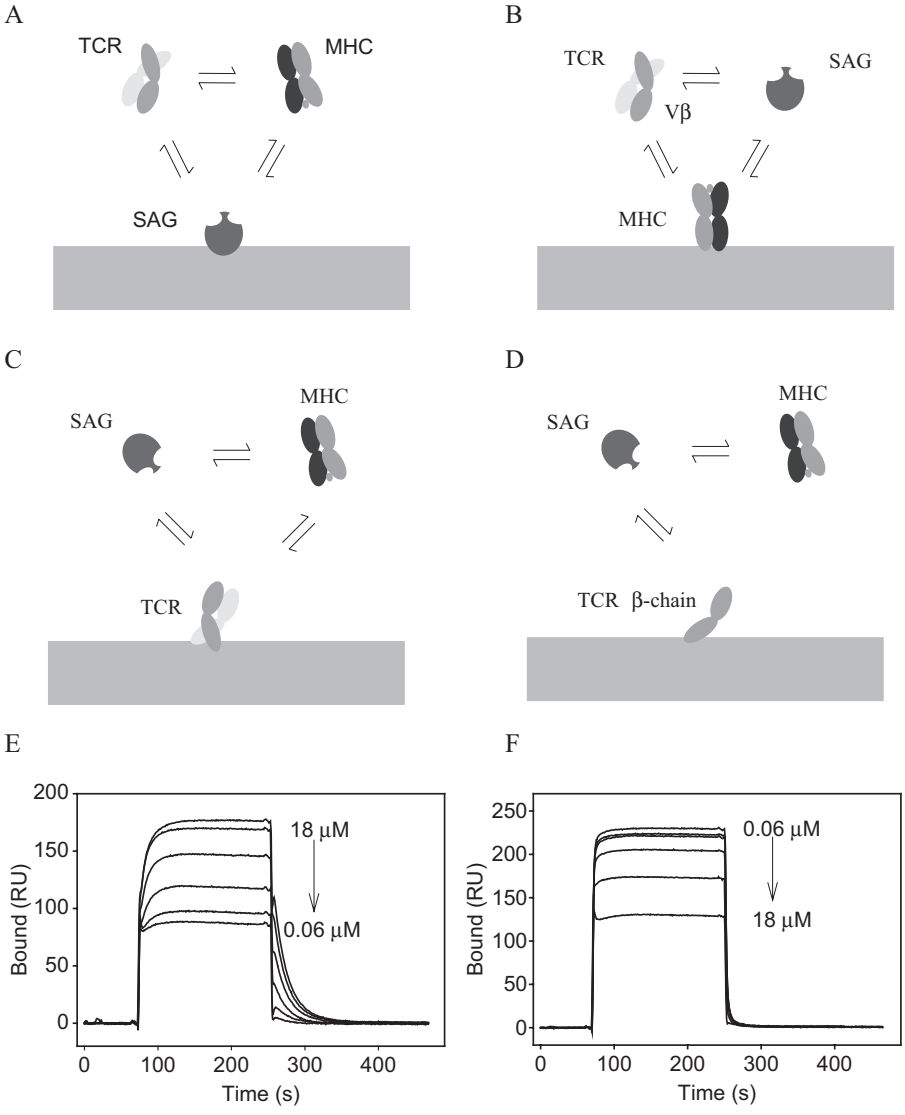

Figure 4.11. (A–D): Possible orientations for studying the interaction between T-cell receptor (TCR) or TCRβ-chain, superantigen (SAG), and major histocompatibility complex (MHC) molecules. (E, F) Positive and negative cooperative effects are involved in ternary complex formation. (E) Overlay sensorgrams of soluble *Staphylococcus* enterotoxin C3 (SEC3) (3.8 μM) binding to immobilized TCRαβ heterodimer in the presence of increasing concentrations of DR1 (0.06, 0.18, 0.60, 1.8, 6.0, and 18 μM as indicated). (B) SEC3 and DR1 binding to immobilized TCRβ-chain. Concentrations of SEC3 and DR1 are as in (E).

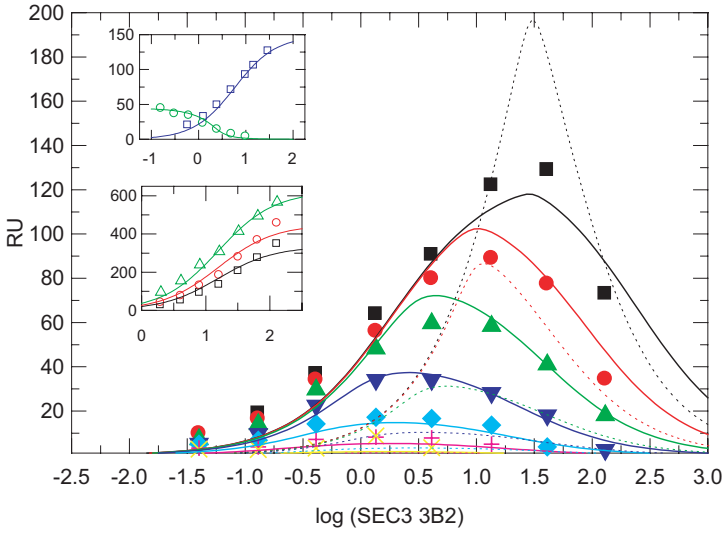

Figure 4.12. Fitting of ternary complex binding results. Representative plots of the global fitting procedure. Solid lines are calculated best-fit isotherms for a model including cooperative binding. For comparison, dotted lines represent the best-fit isotherms calculated in the absence of cooperative binding. Amount of ternary complex formed on immobilized TCRαβ heterodimer using varying concentrations of *Staphylococcus* enterotoxin C3 (SEC3) mixed with DR1 at 30 μM (black squares), 9.5 μM (red circles), 3.0 μM (green triangles), 1.0 μM (blue trangles), 0.3 μM (light blue diamonds), 0.1 μM (purple crosses), and 0.03 μM (yellow crosses). These isotherms reflect the ratio of free SEC3 to SEC3–DR1 complex in solution offered to the immobilized TCRαβ heterodimer. At a fixed concentration of DR1, increasing SEC3 leads to higher SEC3–DR1 complex concentrations available for ternary surface complex formation. At SEC3 concentrations higher than an optimal value, most surface sites will be occupied with unliganded SEC3. The data shown in the insets contain the information on the binary SEC3–T-cell receptor (TCR) and SEC3–DR1 interactions. Upper insert shows dilutions of DR1 binding to immobilized SEC3 (blue squares) and dilutions of SEC3 competing out binding of DR1 to immobilized SEC3 (green circles). Lower insert shows binding of SEC3 to two TCRαβ heterodimer coupled surfaces (red circles and black squares) and one TCRβ surface (green triangles). Reproduced from Andersen *et al.* (2002) with permission.

determined by fitting equilibrium-binding data to a competition model (Figure 4.12, upper insert, in green), using Eq. (4.5). Determination of their solution-binding constant enables the confident prediction of the relative abundance of soluble SEC3–DR1 complexes in the samples used for the study of the ternary complex formation.

The ternary complex formation was explored by acquiring binding data of mixtures of soluble SEC3 and soluble MHC interacting with either surface-immobilized TCRαβ heterodimers, surface-immobilized TCRβ-chains, or blank sensor surfaces (for correcting the signals for contributions arising from the refractive index difference of the sample plugs from the running buffer). SEC3–DR1 mixtures were applied covering a range of concentrations and molar ratios.

To quantify the interaction, a two-dimensional binding isotherm was constructed from the binding data (Figure 4.12). Because the dissociation of SEC3 from TCRαβ heterodimers (in the absence of DR1) was much faster than the dissociation of the ternary complex, and because the DR1 did not bind to the TCR surfaces, the amount of ternary complex formed on TCRαβ heterodimer-coupled surfaces could be estimated from the dissociation phases by extrapolation to the start of the dissociation phase using the known half-life of the ternary complex of 22 s. In contrast, for the surface with the TCRβ-chain, the ternary complex dissociated much faster (Andersen *et al*., 1999) and such a selective observation as for triple protein complex was not possible. Instead, the total surface binding at equilibrium was recorded at the end of the association phase for each mixture of SEC3 and DR1.

The final data sets consisted of 199 and 135 unique data points from the binary- and the ternary-binding isotherms, respectively. These data were subjected to global analysis, using the formulas for the binary surface binding and solution competition isotherms, Eqs (4.3) and (4.5), respectively, and the triple complex isotherm introduced earlier in Eq. (4.11). The parameters included the equilibrium association constant $K_{D,S(surf)}$ for the titration of immobilized SEC3 with soluble DR1, the solution interaction constant $K_{D,S}$ between soluble SEC3 and DR1 in the competition experiment, the binding constant $K_{S,T}$ of soluble SEC3 with immobilized TCR, and the binding constant $K_{DS,T}$ of the preformed soluble DR1–SEC3 complex to immobilized TCR.

Results are presented in Table 4.1 for both αβTCR heterodimers and TCRβ-chains. We found the overall free energy change due to cooperative binding ($\Delta G_{\alpha\beta}$)

Table 4.1. Summary of binding constants

	Unit	SEC3	SEC3
Previous estimates			
$K_{D(SEC3/TCR)}$	μM	22*	–
$K_{D(imm.\ SEC3\ or\ SEC3/sol.\ DR1)}$	μM	270*	4.6*
Independent fits—bimolecular interactions			
$K_{D(SEC3/TCR)}$	μM	–	18 ± 2
$K_{D(imm\ SEC3/sol.\ DR1)}$	μM	–	4.3 ± 1.4
$K_{D(sol.SEC3/sol.\ DR1)}$	μM	–	0.26 ± 0.07
Global fits of ternary complex—bimolecular interactions			
$K_{D(SEC3/TCR)}$	μM	–	22 ± 7
$K_{D(imm\ SEC3/sol.\ DR1)}$	μM	–	4.3 ± 1.4
$K_{D(sol.\ SEC3/sol.\ DR1)}$	μM	–	1.25 ± 1.0
Global fits of ternary complex–cooperative interactions			
$\Delta G_{\alpha\beta}$	kcal mol^{-1}	–	-1.6 ± 0.3
$\Delta G_{v\beta}$	kcal mol^{-1}	–	0.8 ± 0.3
$\Delta G_{v\alpha}$	kcal mol^{-1}	–	-2.4 ± 0.1

*Data from Andersen *et al*. (2002).

to be -1.6 ± 0.3 kcal mol^{-1}. By removing the TCRα-chain, and thereby disrupting the cooperative basis for ternary complex formation, we measure a significant unfavorable cooperative free energy ($\Delta G_{V\beta}$) of 0.8 ± 0.3 kcal mol^{-1}, which indicates that simultaneous binding of TCR and DR1 to SEC3 has significant energetic costs. Finally, the energetic contribution of the DR1β subunit–TCRα-chain interactions ($\Delta G_{V\alpha} = \Delta G_{\alpha\beta} - \Delta G_{V\beta}$) was estimated to be -2.4 ± 0.1 kcal mol^{-1}. This translates into an $\sim$50-fold increase in SEC3 affinity for TCR as a consequence of favorable cooperative interactions and illustrates the significance of the TCR Vα domain in maintaining the biological activity of SEC3. The higher stability of the ternary complex leads to a lower minimal SEC3 concentration at which the ternary complex can be formed, as well as higher SEC3 concentrations at which self-inhibition (i.e., the competition of free SEC3 with SEC3–MHC complexes for TCR binding) takes place. Thus, as a consequence of cooperative binding, the concentration range over which SEC3 can perform its biological function, that is, cross-linking TCR and MHC molecules on apposing cell surfaces, is expanded.

4.5.2. Temperature-Dependent Binding Analysis

For binary interactions, a full set of thermodynamic parameters may be derived by measuring association and dissociation rates at multiple temperatures. This was shown elegantly using SPR for pMHC–TCR interactions (Boniface *et al*., 1999; Willcox *et al*., 1999; Garcia *et al*., 2001), and has since been used for SAG–TCR interactions (Yang *et al*., 2003). Estimates for the enthalpy, entropy, and heat capacity of binding can be derived from the van't Hoff analysis of affinity as a function of temperature. Further, Arrhenius plots of $\ln k_a$ or $\ln k_d$ versus $1/T$ determines the slope of the curve from which the enthalpies of association ($\Delta H_a^{\ddagger}$) and dissociation ($\Delta H_d^{\ddagger}$), respectively, can be determined. These, in turn, provide the activation energies of the interaction, where $\Delta H_a^{\ddagger} = -E_a^{(ass)} - RT$, $\Delta H_d^{\ddagger} = -E_a^{(diss)} - RT$, and $\Delta H^{\ddagger} = \Delta H_a^{\ddagger} - \Delta H_d^{\ddagger}$. High activation energy values indicate that association and dissociation of the complex are impeded by significant energetic barriers. Large, unfavorable entropic changes upon binding can be explained by conformational changes that result in a decrease in mobility of flexibility of the binding sites (i.e., local folding) or from changes in solvent (i.e., incorporation of ordered water molecules in the molecular interface).

When multiple temperature SPR experiments are performed with great care (i.e., to eliminate any aggregates before injection of the analyte), any nonlinearity of $\ln k_a$ or $\ln k_d$ versus T plots that is observed is indicative of significant changes in heat capacity. For rigid-body associations, changes in heat capacity can often be predicted accurately based on changes in buried surface area upon complex

formation (Spolar and Record, 1994). Large discrepancies between calculated and observed heat capacities indicate that the association likely involves conformational changes. Induced-fit mechanisms may be further supported through dissection of the total entropy changes. ΔS_{assoc} for protein–ligand interactions includes several contributions and can be expressed as $\Delta S_{assoc} = \Delta S_{HE} + \Delta S_{tr} + \Delta S_{other}$, where ΔS_{HE} represents entropy changes from hydrophobic effect, ΔS_{tr} entropy changes from rotational and translational entropies of the molecules, and ΔS_{other} any other entropic effects such as vibrational or conformational entropies. For rigid-body interactions, ΔS_{other} is negligible; for induced-fit mechanisms ΔS_{other} is significantly negative. ΔS_{other} values calculated for processes known to couple local or long-range folding to site-specific binding have been reported, and the number of residues that change conformations upon binding can be estimated (Spolar and Record, 1994). This topic is further explored in Chapter 8 on the extended interface.

Even in the absence of rigorous quantitative description of the interaction, this type of analysis may be used to provide qualitative information on the role of protein flexibility in binding. Thus, to explore if molecular flexibility might be involved in the SEC3-mediated cross-linking of the αβTCR heterodimer and MHC, the binding characteristics of various combinations of these three proteins were analyzed at temperatures ranging from 10°C to 30°C at 4°C intervals (Figure 4.13). Binding of MHC to immobilized SEC3 demonstrated temperature-dependent reaction kinetics, with binding kinetics slowing significantly as the temperature was decreased (Figure 4.13A). The most likely mediators of temperature dependence in the SEC3–MHC interaction are the N-terminal residues of the SEC3 disulfide loop, known to be highly flexible, which align to, and make contact with, an α-helix of the MHC molecule (Sundberg *et al*., 2003). In contrast, the kinetics of SEC3 binding to the αβTCR heterodimer were significantly less temperature dependent (Figure 4.13B). Combining SEC3 and MHC in solution and monitoring for binding to immobilized αβTCR heterodimer (Figure 4.13C) showed a significant change in temperature effects relative to SEC3 binding in the absence of MHC, with the kinetics of this reaction being slower and more highly temperature dependent. This suggests that modes of conformational flexibility still present in the binary complexes may be lost when forming a ternary complex. The increase in temperature dependence of SEC3 binding to the αβTCR heterodimer in the presence of DR1, may be the result of flexibility contributed by the MHCβ subunit–TCRα-chain interface (Figure 4.10C) in the ternary complex. Accordingly, no increase in temperature dependence on binding kinetics is seen in complexes involving only the TCRβ-chain, indicating that SEC3 alone likely does not undergo substantial conformational change upon simultaneous binding to TCR and MHC.

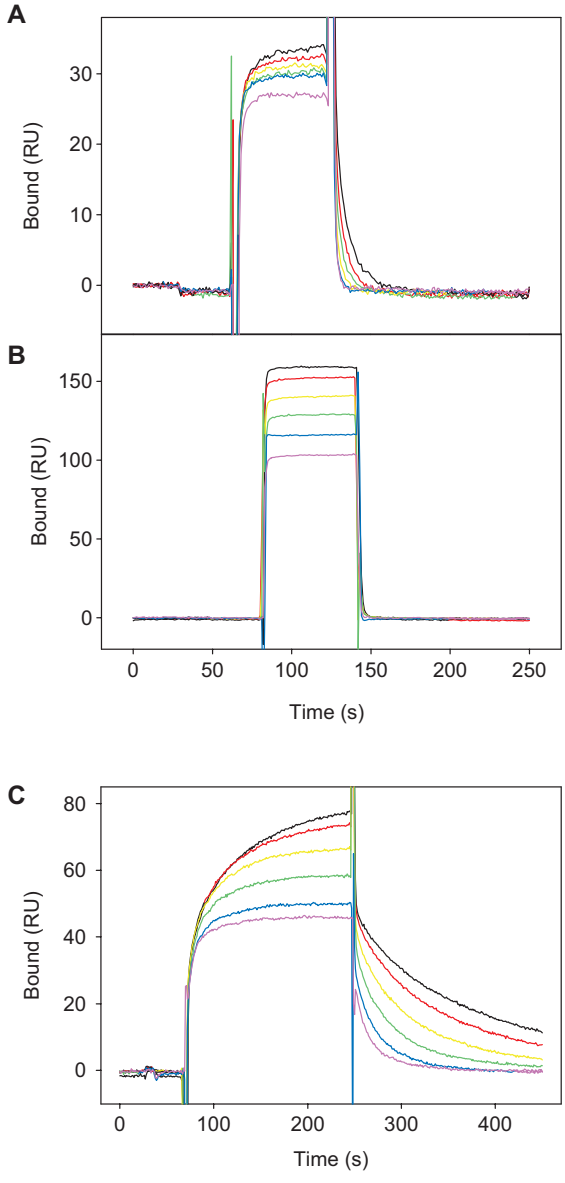

Figure 4.13. The effect of temperature on *Staphylococcus* enterotoxin C3 (SEC3) binding. Overlay sensorgrams of binding reactions at selected equidistant temperatures ranging from 10°C to 30°C. (A) Binding of 8 μM DR1 to immobilized SEC3. (B) Binding of 20 μM SEC3 to immobilized TCRαβ heterodimer. (C) Mixture of 4 μM SEC3 and 3 μM DR1 binding to immobilized TCRαβ heterodimer. Colors of sensorgram traces are as follows: 10°C, black; 14°C, red; 18°C, yellow; 22°C, green; 26°C, blue; and 30°C, magenta. Reproduced from Andersen *et al*. (2002) with permission (we correct the color label of the legend).

4.6. CONCLUSIONS

SPR biosensing can be a very powerful tool in the study of multiprotein complexes and protein interactions involving multiple conformational states. This is amply demonstrated by the numerous examples in the literature of well-controlled studies, where SPR biosensing provided unique insights into the kinetics and the thermodynamics of triple and higher-order protein complexes, revealing cooperativity of binding and details such as the contribution of protein flexibility to the binding process.

SPR biosensing is an extremely versatile approach. Due to the diversity of systems of interacting proteins and the configurations used in their study as described in the literature, we have not provided a systematic account, but tried only to highlight promising opportunities for study. However, as illustrated in the in-depth application to the TCR–MHC–SAG interaction, only particular experimental approaches may appear practical for a given system. For multiprotein interactions, particularly attractive are the configurations exploiting the temporary purification of binary complex through reversible analyte capture, which provide important opportunities for quantitative study. Another advantageous feature of SPR biosensing is the comparatively low amount of material required, even though a well-controlled study may frequently require auxiliary application of other biophysical and biochemical techniques (such as size-exclusion chromatography) with higher protein consumption. Like most biophysical techniques, SPR biosensing also gains in strength considerably when conducted in parallel with other techniques, in particular for elucidating complex-binding reactions. For example, this includes combinations with analytical ultracentrifugation (to study oligomeric state of analyte proteins, and to provide complementary information on the number and stoichiometry of complexes, as well as solution-binding constants for moderate to weak interactions), isothermal titration calorimetry (providing orthogonal thermodynamic information in free solution), and CD (for the study of conformational changes upon binding).

With the technology maturing, critical knowledge has been accumulated about how to conduct reliable studies, including the requirements to generate data with sufficient information content, the nature of potential artifacts, and the potential pitfalls of unquestioned idealizing assumptions, all factors that may lead to quantitatively and qualitatively wrong conclusions if unrecognized. It also has become apparent that SPR shares analytical problems with many other techniques that deal with the analysis of smoothly increasing or decreasing exponential data sets. As a consequence, configurations appear advantageous when different qualitative features of the protein interaction correspond to qualitative features of the recorded binding traces, rather than details in the quantitative analysis (since even though the latter may be very reproducible, this does not necessarily imply that they can be reliably interpreted).

Many of the current limitations are related to the frequently unknown microenvironment of the protein at the surface, and to the fact that a single type of

binding signal is the only source of information to probe the immobilized protein and the interaction. New developments may enable the extension to technology with multiple signals reporting with multiple evanescent fields (and sensitivity). This includes, for example, dual-color SPR (Zacher and Wischerhoff, 2002), use of waveguides (Lukosz, 1991; Salamon *et al*., 1998; Cross *et al*., 2003; Alves *et al*., 2004), combination with fluorescence detection (Liebermann and Knoll, 2000), and many other optical detection approaches (Gauglitz, 2005). It may also be combined with lateral resolution, such as in SPR microscopy (Rothenhäusler and Knoll, 1988; Shumaker-Parry and Campbell, 2004). That a large fraction or even a majority of binding progress is transport limited shows that the sensing technology has to be accompanied with an efficient mass transfer mechanism to further optimize the utility of this method in the study of proteins interactions. An example for a related biosensor approach exploiting multiple detection methods can be found in Chapter 3.

ACKNOWLEDGMENT

We thank Dr Raimund Ober for critically reading the manuscript.

REFERENCES

Abrantes, M., Magone, M. T., Boyd, L. F., and Schuck, P. (2001). Adaptation of the Biacore X surface plasmon resonance biosensor for use with small sample volumes and long contact times. *Anal Chem* 73:2828–2835.

Alves, I. D., Cowell, S. M., Salamon, Z., Devanathan, S., Tollin, G., and Hruby, V. J. (2004). Different structural states of the proteolipid membrane are produced by ligand binding to the human delta-opioid receptor as shown by plasmon-waveguide resonance spectroscopy. *Mol Pharmacol* 65:1248–1257.

Alves, I. D., Park, C. K., and Hruby, V. J. (2005). Plasmon resonance methods in GPCR signaling and other membrane events. *Curr Protein Pept Sci* 6:293–312.

Andersen, P. S., Lavoie, P. M., Sekaly, R. P., Churchill, H., Kranz, D. M., Schlievert, P. M., Karjalainen, K., and Mariuzza, R. A. (1999). Role of the T cell receptor alpha chain in stabilizing TCR–superantigen–MHC class II complexes. *Immunity* 10:473–483.

Andersen, P. S., Schuck, P., Sundberg, E. J., Geisler, C., Karjalainen, K., and Mariuzza, R. A. (2002). Quantifying the energetics of cooperativity in a ternary protein complex. *Biochemistry* 41:5177–5184.

Atanasov, V., Knorr, N., Duran, R. S., Ingebrandt, S., Offenhausser, A., Knoll, W., and Koper, I. (2005). Membrane on a chip: a functional tethered lipid bilayer membrane on silicon oxide surfaces. *Biophys J* 89:1780–1788.

Beattie, J., Phillips, K., Shand, J. H., Szymanowska, M., Flint, D. J., and Allan, G. J. (2005). Molecular recognition characteristics in the insulin-like growth factor (IGF)-insulin-like growth factor binding protein-3/5 (IGFBP-3/5) heparin axis. *J Mol Endocrinol* 34:163–175.

Bernat, B., Pal, G., Sun, M., and Kossiakoff, A. A. (2003). Determination of the energetics governing the regulatory step in growth hormone-induced receptor homodimerization. *Proc Natl Acad Sci USA* 100:952–957.

Bogan, A. A. and Thorn, K. S. (1998). Anatomy of hot spots in protein interfaces. *J Mol Biol* 280:1–9.

Bohach, G. A., Fast, D. J., Nelson, R. D., and Schlievert, P. M. (1990). Staphylococcal and streptococcal pyrogenic toxins involved in toxic shock syndrome and related illnesses. *Crit Rev Microbiol* 17:251–272.

Boniface, J. J., Reich, Z., Lyons, D. S., and Davis, M. M. (1999). Thermodynamics of T cell receptor binding to peptide-MHC: evidence for a general mechanism of molecular scanning. *Proc Natl Acad Sci U S A* 96:11446–11451.

Brecht, A. and Gauglitz, G. (1995). Optical probes and transducers. *Biosens Bioelectron* 10:923–936.

Chen, Z., Earl, P., Damon, I., Zhou, Y.-H., Yu, F., Sebrell, A., Emerson, S., Americo, J., Cohen, G. H., Svitel, J., Schuck, P., Satterfield, W., Moss, B., and Purcell, R. (2006). A chimpanzee monoclonal antibody to vaccinia virus B5R protein protects mice against virulent vaccinia virus and neutralizes vaccinia and smallpox viruses in vitro. *J Infect Dis* 193:625–633.

Cohen, P., Simon, D., Badouaille, G., Mani, J. C., Portefaix, J. M., and Pau, B. (1995). New monoclonal antibodies directed against the propart segment of human prorenin as a tool for the exploration of prorenin conformation. *J Immunol Methods* 184:91–100.

Cooper, M. A. (2002). Optical biosensors in drug discovery. *Nat Rev Drug Discov* 1:515–528.

Cornell, B. A., Krishna, G., Osman, P. D., Pace, R. D., and Wieczorek, L. (2001). Tethered-bilayer lipid membranes as a support for membrane-active peptides. *Biochem Soc Trans* 29:613–617.

Courey, A. J. (2001). Cooperativity in transcriptional control. *Curr Biol* 11:R250–R252.

Crank, J. (1975). *The Mathematics of Diffusion*. Clarendon Press, Oxford.

Cross, G. H., Reeves, A. A., Brand, S., Popplewell, J. F., Peel, L. L., Swann, M. J., and Freeman, N. J. (2003). A new quantitative optical biosensor for protein characterisation. *Biosens Bioelectron* 19:383–390.

Cunningham, B. C. and Wells, J. A. (1993). Comparison of a structural and a functional epitope. *J Mol Biol* 234.

Dallmann, H. G. and McHenry, C. S. (1995). DnaX complex of *Escherichia coli* DNA polymerase III holoenzyme. *J Biol Chem* 270:29563–29569.

Davis, S. J., Ikemizu, S., Wild, M. K., and van der Merwe, P. A. (1998). CD2 and the nature of protein interactions mediating cell–cell recognition. *Immunol Rev* 163:217–236.

De Crescenzo, G., Grothe, S., Lortie, R., Debanne, M. T., and O'Connor-McCourt, M. (2000). Real-time kinetic studies on the interaction of transforming growth factor alpha with the epidermal growth factor receptor extracellular domain reveal a conformational change model. *Biochemistry* 39:9466–9476.

Dubs, M.-C., Altschuh, D., and VanRegenmortel, M. H. V. (1992). Mapping of viral epitopes with conformationally specific monoclonal antibodies using biosensor technology. *J Chromatogr* 597:391–396.

Fägerstam, L. G., Frostell, Å., Karlsson, R., Kullman, M., Larsson, A., Malmqvist, M., and Butt, H. (1990). Detection of antigen–antibody interactions by surface plasmon resonance. Application to epitope mapping. *J Mol Recognit* 3:208–214.

Fields, B. A., Malchiodi, E. L., Li, H., Ysern, X., Stauffacher, C. V., Schlievert, P. M., Karjalainen, K., and Mariuzza, R. A. (1996). Crystal structure of a T-cell receptor beta-chain complexed with a superantigen. *Nature* 384:188–192.

Fischer, P. B., Karlsson, G. B., Butters, T. D., Dwek, R. A., and Platt, F. M. (1996). *N*-butyldeoxynojirimycin-mediated inhibition of human immunodeficiency virus entry correlates with changes in antibody recognition of the V1/V2 region of gp120. *J Virol* 70:7143–7152.

Fong, C.-C., Wong, M.-S., Fong, W.-F., and Yang, M. (2002). Effect on hydrogel matrix on binding kinetics of protein–protein interactions on the sensor surface. *Anal Chim Acta* 456:201–208.

Garcia, K. C., Degano, M., Stanfield, R. L., Brunmark, A., Jackson, M. R., Peterson, P. A., Teyton, L., and Wilson, I. A. (1996). An alpha beta T cell receptor structure at 2.5 A and its orientation in the TCR–MHC complex. *Science* 274:209–219.

Garcia, K. C., Radu, C. G., Ho, J., Ober, R. J., and Ward, E. S. (2001). Kinetics and thermodynamics of T cell receptor–autoantigen interactions in murine experimental autoimmune encephalomyelitis. *Proc Natl Acad Sci USA* 98:6818–6823.

Garland, P. B. (1996). Optical evanescent wave methods for the study of biomolecular interactions. *Q Rev Biophys* 29:91–117.

Gascoigne, N. R. and Ames, K. T. (1991). Direct binding of secreted T-cell receptor beta chain to superantigen associated with class II major histocompatibility complex protein. *Proc Natl Acad Sci USA* 88:613–616.

Gauglitz, G. (2005). Direct optical sensors: principles and selected applications. *Anal Bioanal Chem* 381:141–155.

Gavin, A. C., Bosche, M., Krause, R., Grandi, P., Marzioch, M., Bauer, A., Schultz, J., Rick, J. M., Michon, A. M., Cruciat, C. M., Remor, M., Hofert, C., Schelder, M., Brajenovic, M., Ruffner, H., Merino, A., Klein, K., Hudak, M., Dickson, D., Rudi, T., Gnau, V., Bauch, A., Bastuck, S., Huhse, B., Leutwein, C., Heurtier, M. A., Copley, R. R., Edelmann, A., Querfurth, E., Rybin, V., Drewes, G., Raida, M., Bouwmeester, T., Bork, P., Seraphin, B., Kuster, B., Neubauer, G., and Superti-Furga, G. (2002). Functional organization of the yeast proteome by systematic analysis of protein complexes. *Nature* 415:141–147.

Germain, R. N. and Stefanova, I. (1999). The dynamics of T cell receptor signaling: complex orchestration and the key roles of tempo and cooperation. *Annu Rev Immunol* 17:467–522.

Gilligan, J. J., Schuck, P., and Yergey, A. L. (2002). Mass spectrometry after capture and small-volume elution of analyte from a surface plasmon resonance biosensor. *Anal Chem* 74:2041–2047.

Giot, L., Bader, J. S., Brouwer, C., Chaudhuri, A., Kuang, B., Li, Y., Hao, Y. L., Ooi, C. E., Godwin, B., Vitols, E., Vijayadamodar, G., Pochart, P., Machineni, H., Welsh, M., Kong, Y., Zerhusen, B., Malcolm, R., Varrone, Z., Collis, A., Minto, M., Burgess, S., McDaniel, L., Stimpson, E., Spriggs, F., Williams, J., Neurath, K., Ioime, N., Agee, M., Voss, E., Furtak, K., Renzulli, R., Aanensen, N., Carrolla, S., Bickelhaupt, E., Lazovatsky, Y., DaSilva, A., Zhong, J., Stanyon, C. A., Finley, R. L. Jr., White, K. P., Braverman, M., Jarvie, T., Gold, S., Leach, M., Knight, J., Shimkets, R. A., McKenna, M. P., Chant, J., and Rothberg, J. M. (2003). A protein interaction map of *Drosophila melanogaster*. *Science* 302:1727–1736.

Glaser, R. W. (1993). Antigen–antibody binding and mass transport by convection and diffusion to a surface: a two-dimensional computer model of binding and dissociation kinetics. *Anal Biochem* 213:152–161.

Glaser, R. W. and Hausdorf, G. (1996). Binding kinetics of an antibody against HIV p24 core protein measured with real-time biomolecular interaction analysis suggest a slow conformational change in antigen p24. *J Immunol Methods* 189:1–14.

Greenfield, C., Hiles, I., Waterfield, M. D., Federwisch, M., Wollmer, A., Blundell, T. L., and McDonald, N. (1989). Epidermal growth factor binding induces a conformational change in the external domain of its receptor. *Embo J* 8:4115–4123.

Hall, D. (2001). Use of optical biosensors for the study of mechanistically concerted surface adsorption processes. *Anal Biochem* 288:109–125.

Hall, D. R., Cann, J. R., and Winzor, D. J. (1996). Demonstration of an upper limit to the range of association rate constants amenable to study by biosensor technology based on surface plasmon resonance. *Anal Biochem* 235:175–184.

Hanisch, F. G., Uhlenbruck, G., Egge, H., and Peter-Katalinic, J. (1989). A B72.3 second-generation-monoclonal antibody (CC49) defines the mucin-carried carbohydrate epitope Gal beta(1–3) [NeuAc alpha(2–6)]GalNAc. *Biol Chem Hoppe Seyler* 370:21–26.

Hansen, P. C. (1998). *Rank-Deficient and Discrete Ill-Posed Problems: Numerical Aspects of Linear Inversion*. SIAM, Philadelphia.

Hasegawa, K., Ono, K., Yamada, M., and Naiki, H. (2002). Kinetic modeling and determination of reaction constants of Alzheimer's beta-amyloid fibril extension and dissociation using surface plasmon resonance. *Biochemistry* 41:13489–13498.

Ho, Y., Gruhler, A., Heilbut, A., Bader, G. D., Moore, L., Adams, S. L., Millar, A., Taylor, P., Bennett, K., Boutilier, K., Yang, L., Wolting, C., Donaldson, I., Schandorff, S., Shewnarane, J., Vo, M., Taggart, J., Goudreault, M., Muskat, B., Alfarano, C., Dewar, D., Lin, Z., Michalickova, K., Willems, A. R., Sassi, H., Nielsen, P. A., Rasmussen, K. J., Andersen, J. R., Johansen, L. E.,

Hansen, L. H., Jespersen, H., Podtelejnikov, A., Nielsen, E., Crawford, J., Poulsen, V., Sorensen, B. D., Matthiesen, J., Hendrickson, R. C., Gleeson, F., Pawson, T., Moran, M. F., Durocher, D., Mann, M., Hogue, C. W., Figeys, D., and Tyers, M. (2002). Systematic identification of protein complexes in *Saccharomyces cerevisiae* by mass spectrometry. *Nature* 415:180–183.

Honjo, E., Watanabe, K., and Tsukamoto, T. (2002). Real-time kinetic analyses of the interaction of ricin toxin A-chain with ribosomes prove a conformational change involved in complex formation. *J Biochem* (*Tokyo*) 131:267–275.

Huber, A., Demartis, S., and Neri, D. (1999). The use of biosensor technology for the engineering of antibodies and enzymes. *J Mol Recognit* 12:198–216.

Ibrahimi, O. A., Zhang, F., Hrstka, S. C., Mohammadi, M., and Linhardt, R. J. (2004). Kinetic model for FGF, FGFR, and proteoglycan signal transduction complex assembly. *Biochemistry* 43:4724–4730.

Ito, T., Chiba, T., Ozawa, R., Yoshida, M., Hattori, M., and Sakaki, Y. (2001). A comprehensive two-hybrid analysis to explore the yeast protein interactome. *Proc Natl Acad Sci USA* 98:4569–4574.

Johnsson, B., Löfås, S., and Lindquist, G. (1991). Immobilization of proteins to a carboxymethyldextran-modified gold surface for biospecific interaction analysis in surface plasmon resonance sensors. *Anal Biochem* 198:268–277.

Jönsson, U. and Malmqvist, M. (1992). Real time biospecific interaction analysis. *Adv Biosens* 2:291–336.

Joss, L., Morton, T. A., Doyle, M. L., and Myszka, D. G. (1998). Interpreting kinetic rate constants from optical biosensor data recorded on a decaying surface. *Anal Biochem* 261:203–210.

Karlsson, R. (1994). Real-time competitive kinetic analysis of interactions between low-molecular-weight ligands in solution and surface-immobilized receptors. *Anal Biochem* 221:142–151.

Karlsson, R. and Fält, A. (1997). Experimental design for kinetic analysis of protein–protein interactions with surface plasmon resonance biosensors. *J Immunol Methods* 200:121–133.

Karlsson, R., Michaelsson, A., and Mattson, L. (1991). Kinetic analysis of monoclonal antibody–antigen interactions with a new biosensor based analytical system. *J Immunol Methods* 145:229–240.

Karlsson, R., Roos, H., Fägerstam, L., and Persson, B. (1994). Kinetic and concentration analysis using BIA technology. *Methods: A Companion to Methods Enzymol* 6:99–110.

Karp, N. A., Edwards, P. R., and Leatherbarrow, R. J. (2005). Analysis of calibration methodologies for solvent effects in drug discovery studies using evanescent wave biosensors. *Biosens Bioelectron* 21:128–134.

Khursigara, C. M., De Crescenzo, G., Pawelek, P. D., and Coulton, J. W. (2005). Kinetic analyses reveal multiple steps in forming TonB–FhuA complexes from *Escherichia coli*. *Biochemistry* 44:3441–3453.

Knoll, W. (1998). Interfaces and thin films as seen by bound electromagnetic waves. *Annu Rev Phys Chem* 49:569–638.

Kotzin, B. L., Leung, D. Y., Kappler, J., and Marrack, P. (1993). Superantigens and their potential role in human disease. *Adv Immunol* 54:99–166.

Kretschmann, E. and Raether, H. (1968). Radiative decay of non-radiative surface plasmons excited by light. *Z Naturforsch* 23a:2135–2136.

Krone, J. R., Nelson, R. W., Dogruel, D., Williams, P., and Granzow, R. (1997). BIA/MS: interfacing biomolecular interaction analysis with mass spectrometry. *Anal Biochem* 244:124–132.

Ladbury, J. E., Lemmon, M. A., Zhou, M., Green, J., Botfield, M. C., and Schlesinger, J. (1995). Measurement of the binding of tyrosyl phosphopeptides to SH2 domains: a reappraisal. *Proc Natl Acad Sci USA* 92:3199–3203.

Langmuir, I. (1918). The adsorption of gases on plane surfaces of glass, mica and platinum. *J Am Chem Soc* 40:1361–1403.

Lata, S. and Piehler, J. (2005). Stable and functional immobilization of histidine-tagged proteins via multivalent chelator head groups on a molecular poly(ethylene glycol) brush. *Anal Chem* 77:1096–1105.

Lee, H. J., Yan, Y., Marriott, G., and Corn, R. M. (2005). Quantitative functional analysis of protein complexes on surfaces. *J Physiol* 563:61–71.

Li, S., Armstrong, C. M., Bertin, N., Ge, H., Milstein, S., Boxem, M., Vidalain, P. O., Han, J. D., Chesneau, A., Hao, T., Goldberg, D. S., Li, N., Martinez, M., Rual, J. F., Lamesch, P., Xu, L., Tewari, M., Wong, S. L., Zhang, L. V., Berriz, G. F., Jacotot, L., Vaglio, P., Reboul, J., Hirozane-Kishikawa, T., Li, Q., Gabel, H. W., Elewa, A., Baumgartner, B., Rose, D. J., Yu, H., Bosak, S., Sequerra, R., Fraser, A., Mango, S. E., Saxton, W. M., Strome, S., Van Den Heuvel, S., Piano, F., Vandenhaute, J., Sardet, C., Gerstein, M., Doucette-Stamm, L., Gunsalus, K. C., Harper, J. W., Cusick, M. E., Roth, F. P., Hill, D. E., and Vidal, M. (2004). A map of the interactome network of the metazoan *C. elegans*. *Science* 303:540–543.

Liebermann, T. and Knoll, W. (2000). Surface-plasmon filed-enhanced fluorescence spectroscopy. *Colloids Surf A* 171:115–130.

Lieto, A. M., Cush, R. C., and Thompson, N. L. (2003). Ligand–receptor kinetics measured by total internal reflection with fluorescence correlation spectroscopy. *Biophys J* 85:3294–3302.

Lipschultz, C. A., Li, Y., and Smith-Gill, S. (2000). Experimental design for analysis of complex kinetics using surface plasmon resonance. *Methods* 20:310–318.

Lo Conte, L., Chothia, C., and Janin, J. (1999). The atomic structure of protein–protein recognition sites. *J Mol Biol* 285:2177–2198.

Löfås, S. and Johnsson, B. (1990). A novel hydrogel matrix on gold surfaces in surface plasmon resonance sensors for fast and efficient covalent immobilization of ligands. *J Chem Soc*, *Chem Commun* 21:1526–1528.

Lukosz, W. (1991). Principles and sensitivities of integrated optical and surface plasmon sensors for direct affinity sensing and immunosensing. *Biosens Bioelectron* 6:215–225.

Ma, B., Wolfson, H. J., and Nussinov, R. (2001). Protein functional epitopes: hot spots, dynamics and combinatorial libraries. *Curr Opin Struct Biol* 11:364–369.

Malchiodi, E. L., Eisenstein, E., Fields, B. A., Ohlendorf, D. H., Schlievert, P. M., Karjalainen, K., and Mariuzza, R. A. (1995). Superantigen binding to a T cell receptor beta chain of known three-dimensional structure. *J Exp Med* 182:1833–1845.

Malmborg, A. C. and Borrebaeck, C. A. (1995). BIAcore as a tool in antibody engineering. *J Immunol Methods* 183:7–13.

McCraith, S., Holtzman, T., Moss, B., and Fields, S. (2000). Genome-wide analysis of vaccinia virus protein–protein interactions. *Proc Natl Acad Sci USA* 97:4879–4884.

Mehlmann, M., Garvin, A. M., Steinwand, M., and Gauglitz, G. (2005). Reflectometric interference spectroscopy combined with MALDI-TOF mass spectrometry to determine quantitative and qualitative binding of mixtures of vancomycin derivatives. *Anal Bioanal Chem* 382:1942–1948.

Morton, T. A., Myszka, D. G., and Chaiken, I. M. (1995). Interpreting complex binding kinetics from optical biosensors: a comparison of analysis by linearization, the integrated rate equation, and numerical integration. *Anal Biochem* 227:176–185.

Muller, K. M., Arndt, K. M., and Pluckthun, A. (1998). Model and simulation of multivalent binding to fixed ligands. *Anal Biochem* 261:149–158.

Myszka, D., Arulanantham, P. R., Sana, T., Wu, Z., Morton, T. A., and Ciardelli, T. L. (1996). Kinetic analysis of ligand binding to interleukin-2 receptor complexes created on an optical biosensor surface. *Protein Sci* 5:2468–2478.

Natsume, T., Nakayama, H., Jansson, O., Isobe, T., Takio, K., and Mikoshiba, K. (2000). Combination of biomolecular interaction analysis and mass spectrometric amino acid sequencing. *Anal Chem* 72:4193–4198.

Natsume, T., Yamauchi, Y., Nakayama, H., Shinkawa, T., Yanagida, M., Takahashi, N., and Isobe, T. (2002). A direct nanoflow liquid chromatography-tandem mass spectrometry system for interaction proteomics. *Anal Chem* 74:4725–4733.

Nieba, L., Krebber, A., and Plückthun, A. (1996). Competition BIAcore for measuring true affinities: large differences from values determined from binding kinetics. *Anal Biochem* 234:155–165.

Northup, J. (2004). Measuring rhodopsin-G-protein interactions by surface plasmon resonance. *Methods Mol Biol* 261:93–112.

O'Shannessy, D. J. (1994). Determination of kinetic rate and equilibrium binding constants for macromolecular interactions: a critique of the surface plasmon resonance literature. *Curr Opin Biotechnol* 5:65–71.

O'Shannessy, D. J., Brigham-Burke, M., and Peck, K. (1992). Immobilization chemistries suitable for use in the BIAcore surface plasmon resonance detector. *Anal Biochem* 205:132–136.

O'Shannessy, D. J., Brigham-Burke, M., Soneson, K. K., Hensley, P., and Brooks, I. (1993). Determination of rate and equilibrium binding constants for macromolecular interactions using surface plasmon resonance: use of nonlinear least squares analysis methods. *Anal Biochem* 212:457–468.

Ober, R. J., Caves, J., and Ward, E. S. (2003). Analysis of exponential data using a noniterative technique: application to surface plasmon experiments. *Anal Biochem* 312:57–65.

Ober, R. J. and Ward, E. S. (1999a). The choice of reference cell in the analysis of kinetic data using BIAcore. *Anal Biochem* 271:70–80.

Ober, R. J. and Ward, E. S. (1999b). The influence of signal noise on the accuracy of kinetic constants measured by surface plasmon resonance experiments. *Anal Biochem* 273:49–59.

Parsons, I. D. and Stockley, P. G. (1997). Quantitation of the *Escherichia coli* methionine repressor–operator interaction by surface plasmon resonance is not affected by the presence of a dextran matrix. *Anal Biochem* 254:82–87.

Pattnaik, P. (2005). Surface plasmon resonance: applications in understanding receptor–ligand interaction. *Appl Biochem Biotechnol* 126:79–92.

Piehler, J., Brecht, A., Hehl, K., and Gauglitz, G. (1999). Protein interactions in covalently attached dextran layers. *Colloids Surf B Biointerfaces* 13:325–336.

Plant, A. L., Brigham-Burke, M., Petrella, E. C., and O'Shannessy, D. J. (1995). Phospholipid/alkanethiol bilayers for cell-surface receptor studies by surface plasmon resonance. *Anal Biochem* 226:342–348.

Provencher, S. W. (1982). CONTIN: a general purpose constrained regularization program for inverting noisy linear algebraic and integral equations. *Comput Phys Commun* 27:229–242.

Raether, H. (1977). Surface plasma oscillations and their applications. In: Hass, G., Francombe, M. H., and Hoffman, R. W. (eds), *Physics of Thin Films*, volume 9. Academic Press, New York, pp. 145–261.

Rain, J. C., Selig, L., De Reuse, H., Battaglia, V., Reverdy, C., Simon, S., Lenzen, G., Petel, F., Wojcik, J., Schachter, V., Chemama, Y., Labigne, A., and Legrain, P. (2001). The protein–protein interaction map of *Helicobacter pylori*. *Nature* 409:211–215.

Rao, N. M., Plant, A. L., Silin, V., Wight, S., and Hui, S. W. (1997). Characterization of biomimetic surfaces formed from cell membranes. *Biophys J* 73:3066–3077.

Rebois, R. V., Schuck, P., and Northup, J. K. (2002). Elucidating kinetic and thermodynamic constants for interaction of G protein subunits and receptors by surface plasmon resonance spectroscopy. *Methods Enzymol* 344:15–42.

Reddish, M. A., Jackson, L., Koganty, R. R., Qiu, D., Hong, W., and Longenecker, B. M. (1997). Specificities of anti-sialyl-Tn and anti-Tn monoclonal antibodies generated using novel clustered synthetic glycopeptide epitopes. *Glycoconj J* 14:549–560.

Redpath, S., Alam, S. M., Lin, C. M., O'Rourke, A. M., and Gascoigne, N. R. (1999). Cutting edge: trimolecular interaction of TCR with MHC class II and bacterial superantigen shows a similar affinity to MHC:peptide ligands. *J Immunol* 163:6–10.

Renno, T. and Acha-Orbea, H. (1996). Superantigens in autoimmune diseases: still more shades of gray. *Immunol Rev* 154:175–191.

Roden, L. D. and Myszka, D. G. (1996). Global analysis of a macromolecular interaction measured on BIAcore. *Biochem Biophys Res Commun* 225:1073–1077.

Rosovitz, M. J., Schuck, P., Varughese, M., Chopra, A. P., Mehra, V., Singh, Y., McGinnis, L. M., and Leppla, S. H. (2003). Alanine-scanning mutations in domain 4 of anthrax toxin protective antigen reveal residues important for binding to the cellular receptor and to a neutralizing monoclonal antibody. *J Biol Chem* 278:30936–30944.

Rothenhäusler, B. and Knoll, W. (1988). Surface-plasmon microscopy. *Nature* 332:615–617.

Salamon, Z., Brown, M. F., and Tollin, G. (1999). Plasmon resonance spectroscopy: probing molecular interactions within membranes. *Trends Biochem Sci* 24:213–219.

Salamon, Z., Huang, D., Cramer, W. A., and Tollin, G. (1998). Coupled plasmon-waveguide resonance spectroscopy studies of the cytochrome b6f/plastocyanin system in supported lipid bilayer membranes. *Biophys J* 75:1874–1885.

Salamon, Z., Wang, Y., Brown, M. F., Macleod, H. A., and Tollin, G. (1994). Conformational changes in rhodopsin probed by surface plasmon resonance spectroscopy. *Biochemistry* 33:13706–13711.

Schmelz, M., Sodeik, B., Ericsson, M., Wolffe, E. J., Shida, H., Hiller, G., and Griffiths, G. (1994). Assembly of vaccinia virus: the second wrapping cisterna is derived from the trans Golgi network. *J Virol* 68:130–147.

Schuck, P. (1996). Kinetics of ligand binding to receptor immobilized in a polymer matrix, as detected with an evanescent wave biosensor. I. A computer simulation of the influence of mass transport. *Biophys J* 70:1230–1249.

Schuck, P. (1997a). Reliable determination of binding affinity and kinetics using surface plasmon resonance biosensors. *Curr Opin Biotechnol* 8:498–502.

Schuck, P. (1997b). Use of surface plasmon resonance to probe the equilibrium and dynamic aspects of interactions between biological macromolecules. *Ann Rev Biophys Biomol Struct* 26:541–566.

Schuck, P. (2000). Size distribution analysis of macromolecules by sedimentation velocity ultracentrifugation and Lamm equation modeling. *Biophys J* 78:1606–1619.

Schuck, P., Boyd, L. F., and Andersen, P. S. (1999). Measuring protein interactions by optical biosensors. In: Coligan, J. E., Dunn, B. M., Ploegh, H. L., Speicher, D. W., and Wingfield, P. T. (eds), *Current Protocols in Protein Science*, volume 2. Wiley, New York, pp. 20.2.1–20.2.21.

Schuck, P., Millar, D. B., and Kortt, A. A. (1998). Determination of binding constants by equilibrium titration with circulating sample in a surface plasmon resonance biosensor. *Anal Biochem* 265:79–91.

Schuck, P. and Minton, A. P. (1996). Analysis of mass transport limited binding kinetics in evanescent wave biosensors. *Anal Biochem* 240:262–272.

Schuster, S. C., Swanson, R. V., Alex, L. A., Bourret, R. B., and Simon, M. I. (1993). Assembly and function of a quaternary signal transduction complex monitored by surface plasmon resonance. *Nature* 365:343–347.

Shumaker-Parry, J. S. and Campbell, C. T. (2004). Quantitative methods for spatially resolved adsorption/desorption measurements in real time by surface plasmon resonance microscopy. *Anal Chem* 76:907–917.

Sjölander, S. and Urbaniczky, C. (1991). Integrated fluid handling system for biomolecular interaction analysis. *Anal Chem* 63:2338–2345.

Sonksen, C. P., Nordhoff, E., Jansson, O., Malmqvist, M., and Roepstorff, P. (1998). Combining MALDI mass spectrometry and biomolecular interaction analysis using a biomolecular interaction analysis instrument. *Anal Chem* 70:2731–2736.

Spolar, R. S. and Record, M. T. Jr. (1994). Coupling of local folding to site-specific binding of proteins to DNA. *Science* 263:777–784.

Stenberg, E., Persson, B., Roos, H., and Urbaniczky, C. (1991). Quantitative determination of surface concentration of protein with surface plasmon resonance using radiolabeled proteins. *J Coll Interface Sci* 143:513–526.

Stokes, R. H., Oakhill, J. S., Joannou, C. L., Gorringe, A. R., and Evans, R. W. (2005). Meningococcal transferrin-binding proteins A and B show cooperation in their binding kinetics for human transferrin. *Infect Immun* 73:944–952.

Sundberg, E. J., Andersen, P. S., Schlievert, P. M., Karjalainen, K., and Mariuzza, R. A. (2003). Structural, energetic and functional analysis of a protein–protein interface at distinct stages of affinity maturation. *Structure* 11:1151–1161.

Sundberg, E. J., Li, Y., and Mariuzza, R. A. (2002). So many ways of getting in the way: diversity in the molecular architecture of superantigen-dependent T-cell signaling complexes. *Curr Opin Immunol* 14:36–44.

Sundberg, E. J. and Mariuzza, R. A. (2000). Luxury accommodations: the expanding role of structural plasticity in protein–protein interactions. *Structure Fold Des* 8:R137–R142.

Sundberg, E. J. and Mariuzza, R. A. (2002). Molecular recognition in antigen–antibody complexes. *Adv Protein Chem* 61:119–160.

Svitel, J., Balbo, A., Mariuzza, R. A., Gonzales, N. R., and Schuck, P. (2003). Combined affinity and rate constant distributions of analyte or ligand populations from experimental surface binding and kinetics and equilibria. *Biophys J* 84:4062–4077.

Svitel, J., Boukari, H., Gorshkova, I. I., Sackett, D. L., and Schuck, P. (submitted). Probing the functional heterogeneity of surface binding sites.

Tanaka, M. and Sackmann, E. (2005). Polymer-supported membranes as models of the cell surface. *Nature* 437:656–663.

Uetz, P., Giot, L., Cagney, G., Mansfield, T. A., Judson, R. S., Knight, J. R., Lockshon, D., Narayan, V., Srinivasan, M., Pochart, P., Qureshi-Emili, A., Li, Y., Godwin, B., Conover, D., Kalbfleisch, T., Vijayadamodar, G., Yang, M., Johnston, M., Fields, S., and Rothberg, J. M. (2000). A comprehensive analysis of protein–protein interactions in *Saccharomyces cerevisiae*. *Nature* 403:623–627.

van der Merwe, P. A. and Barclay, A. N. (1996). Analysis of cell-adhesion molecule interactions using surface plasmon resonance. *Curr Opin Immunol* 8:257–261.

van der Merwe, P. A., Barclay, A. N., Mason, D. W., Davies, E. A., Morgan, B. P., Tone, M., Krishnam, A. K. C., Ianelli, C., and Davis, S. J. (1994). Human cell-adhesion molecule CD2 binds CD58 (LFA-3) with a very low affinity and an extremely fast dissociation rate but does not bind CD48 or CD59. *Biochemistry* 33:10149–10160.

Vives, R. R., Sadir, R., Imberty, A., Rencurosi, A., and Lortat-Jacob, H. (2002). A kinetics and modeling study of RANTES(9–68) binding to heparin reveals a mechanism of cooperative oligomerization. *Biochemistry* 41:14779–14789.

Vorup-Jensen, T., Carman, C. V., Shimaoka, M., Schuck, P., Svitel, J., and Springer, T. A. (2005). Exposure of acidic residues as a danger signal for recognition of fibrinogen and other macromolecules by integrin alphaXbeta2. *Proc Natl Acad Sci USA* 102:1614–1619.

Walhout, A. J., Sordella, R., Lu, X., Hartley, J. L., Temple, G. F., Brasch, M. A., Thierry-Mieg, N., and Vidal, M. (2000). Protein interaction mapping in *C. elegans* using proteins involved in vulval development. *Science* 287:116–122.

Walsh, S. T., Jevitts, L. M., Sylvester, J. E., and Kossiakoff, A. A. (2003). Site 2 binding energetics of the regulatory step of growth hormone-induced receptor homodimerization. *Protein Sci* 12:1960–1970.

Willcox, B. E., Gao, G. F., Wyer, J. R., Ladbury, J. E., Bell, J. I., Jakobsen, B. K., and van der Merwe, P. A. (1999). TCR binding to peptide-MHC stabilizes a flexible recognition interface. *Immunity* 10:357–365.

Williams, C. and Addona, T. A. (2000). The integration of SPR biosensors with mass spectrometry: possible applications for proteome analysis. *Trends Biotechnol* 18:45–48.

Winzor, D. J. (2000). From gel filtration to biosensor technology: the development of chromatography for the characterization of protein interactions. *J Mol Recognit* 13:279–298.

Wofsy, C. and Goldstein, B. (2002). Effective rate models for receptors distributed in a layer above a surface: application to cells and Biacore. *Biophys J* 82:1743–1755.

Yang, J., Swaminathan, C. P., Huang, Y., Guan, R., Cho, S., Kieke, M. C., Kranz, D. M., Mariuzza, R. A., and Sundberg, E. J. (2003). Dissecting cooperative and additive binding energetics in the affinity maturation pathway of a protein–protein interface. *J Biol Chem* 278:50412–50421.

Yarmush, M. L., Patankar, D. B., and Yarmush, D. M. (1996). An analysis of transport resistances in the operation of BIAcore; implications for kinetic studies of biospecific interactions. *Mol Immunol* 33:1203–1214.

Yeung, D., Gill, A., Maule, C. H., and Davies, R. J. (1995). Detection and quantification of biomolecular interactions with optical biosensors. *Trends Anal Chem* 14:49–56.

Zacher, T. and Wischerhoff, E. (2002). Real-time two-wavelength surface plasmon resonance as a tool for the vertical resolution of binding processes in biosensing hydrogels. *Langmuir* 18:1748–1759.